N°...../DTEH/2025

REPUBLIQUE ALGERIENNE DEMOCRATIQUE ET POPULAIRE
Ministère de l'enseignement Supérieur et de la Recherche Scientifique

Université M'Hamed Bougara-Boumerdes
Faculté des Hydrocarbures et de la Chimie

Département Transport et Equipements des Hydrocarbures

Mémoire de fin d'études
En vue de l'obtention du diplôme de

Master

Domaine : Sciences et Technologies

Filière : Hydrocarbures

Option : Génie Mécanique : Mécanique des Chantiers Pétroliers

Présenté par : FRADJ Oussama Souheib
TAOUCHE Benyoucef Soufiane

THEME

Assessment of the effect of nitriding treatment on physical and mechanical properties of stainless steels

Devant le jury :

GACEB Mohamed	Prof	UMBB	President
KASSAI I.	MCB	UMBB	Examiner
CHEKIROU F.	MCB	UMBB	Examiner
Chemaa Khaled	MCB	UMBB	Encadreur
Ouahid Sifi	Maitre de Recherche A	CDTA	Co-encadreur

Boumerdes 2024-2025

Dédicaces

Tout d'abord je dédie ce modeste travail à mes très chers parents, pour tout ce qu'ils ont fait afin que je puisse en arriver là, puisse Allah les protège et les garde en bon santé.

Je n'oublierai jamais d'exprimer ma profonde reconnaissance à ma chère tante la Professeure **FRADJ Nasira**, qui a été pour moi un véritable soutien, celle qui a semé en moi l'espoir, et m'a appris que la volonté sincère permet de dépasser toutes les difficultés. Sa main a toujours été tendue vers moi, et son soutien a laissé une empreinte profonde dans mon cœur et dans mon parcours académique.

À ma **mère chaste**, au cœur pur et à l'âme noble, celle qui m'a toujours encouragé(e) par ses paroles réconfortantes et ses larmes précieuses. Par ses prières constantes, elle m'a protégé(e) de tout mal. Elle est le premier pilier de ma vie et la base essentielle de toute réussite que j'ai accomplie et que j'accomplirai, si Dieu le veut. Je prie le Très-Haut de la préserver et de la garder en bonne santé parmi nous.

À mes chers frères **Mossab**, **Somia**, **Youcef** et **Hiba**. À toute ma famille. À tous mes amis et collègues À tous ceux qui m'ont aidé de près ou de loin. Enfin à tous ceux que j'aime et qui m'aiment

Souheib

Dédicaces

Je dédie ce modeste travail : À mes chers parents « TAOUCHE MEHAMED & GUENDA FATIMA », pour tous leurs sacrifices, leur amour, leur tendresse, leur soutien et leurs prières tout au long de mes études,

À mes chères sœurs « HIBA & AYA & MARWA » pour leurs encouragements permanents, et leur soutien moral,

À mon cher frère « ABDEL SAMID » pour leur appui et leur encouragement, À mon binôme « fradj oussama »,

À toute ma famille pour son soutien tout au long de mon parcours universitaire, À mes très chères amies,

Que ce travail soit l'accomplissement de nos vœux tant allégués.

SOUFIANE

Remerciements

Tout d’abord, je remercie le bon dieu, le tout puissant pour avoir me donner la volonté, la santé et la patience, qui m'ont permis d’accomplir ce travail modeste et d’atteindre les objectifs que je m’étais fixés. Je Le remercie également pour avoir facilité ma vie et ma subsistance

Avec toute ma reconnaissance et ma considération, j’exprime ma profonde gratitude à toutes les personnes qui m’ont soutenu et accompagné, que ce soit par leurs conseils, leur soutien moral ou leurs contributions scientifiques directes, tout au long de la préparation de ce travail de recherche.

J’adresse mes plus sincères remerciements à **Monsieur CHAMAA Khaled**, mon encadrant respecté, pour avoir accepté de superviser ce travail, pour les efforts qu’il a déployés afin de me guider, ainsi que pour son soutien constant. Sa confiance, ses encouragements et ses précieux conseils ont eu un impact déterminant sur la réalisation de ce projet.

Je tiens également à exprimer ma profonde reconnaissance à **Monsieur SIFI Ouahid**, qui a proposé le sujet de ce mémoire et m’a accompagné tout au long de son élaboration grâce à sa grande expertise scientifique et à ses qualités humaines remarquables. Il m’a offert une opportunité précieuse de travailler en autonomie, ce qui m’a permis de vivre une expérience de recherche enrichissante dans un domaine à forte technicité. Ce fut un réel plaisir de collaborer avec lui durant toute la durée de ce travail.

Je remercie également l’ensemble du personnel de la **Division des milieux ionisés et lasers** du **Centre de Développement des Technologies Avancées (CDTA)**, pour les facilités et les connaissances mises à ma disposition. J’adresse une mention particulière à **Monsieur Amine**, pour son professionnalisme, sa coopération, et ses contributions précieuses qui ont enrichi ce travail.

Enfin, je n’oublie pas de remercier toutes les personnes qui m’ont soutenu et tendu la main, de près ou de loin, tout au long de ce projet.

Abstract

The aim of this study is to apply a low-temperature plasma nitriding to AISI 304 and 316L stainless steels to evaluate its impact on structural, mechanical, and electrochemical properties. X-ray diffraction (XRD) confirmed the formation of expanded austenite (γN), which is responsible for the hardness improvement. Nanoindentation tests showed a reduction in penetration depth from ~1150 to 1100 nm in 304 and from ~1100 to 1070 nm in 316L under a 100 mN load. Electrochemical analysis revealed divergent behaviors. In AISI 304, corrosion resistance decreased significantly, with corrosion potential shifting from –28.7 to –306.9 mV and corrosion current density rising from 7.76 nA to 3.97 µA. This deterioration is attributed to unstable passive films and microstructural discontinuities caused by heterogeneous nitrogen saturation. In contrast, AISI 316L exhibited improved corrosion behavior: despite an increase in current density from 10.5 nA to 6.69 µA, impedance spectroscopy confirmed a strong capacitive response, indicating the formation of a more stable and homogeneous γN layer. The presence of molybdenum in 316L played a key role in enhancing passive film stability. These results indicate that plasma nitriding improved hardness in both alloys through interstitial nitrogen strengthening but affected corrosion differently depending on alloy composition: degradation in 304 due to passive film instability, and reinforcement in 316L thanks to molybdenum's stabilizing effect.

Keywords: Stainless Steel ; AISI 316L ; AISI 304 ; Hardness ; Corrosion ; Plasma Nitriding.

Résumé

L'objectif de cette étude est d'appliquer une nitruration par plasma à basse température sur les aciers inoxydables AISI 304 et 316L afin d'évaluer son impact sur les propriétés structurelles, mécaniques et électrochimiques. La diffraction des rayons X (DRX) a confirmé la formation de l'austénite élargie (γN), responsable de l'amélioration de la dureté. Les tests de nanoindentation ont montré une réduction de la profondeur de pénétration de ~1150 à 1100 nm pour le 304 et de ~1100 à 1070 nm pour le 316L sous une charge de 100 mN. L'analyse électrochimique a révélé des comportements divergents. Pour l'AISI 304, la résistance à la corrosion a diminué de manière significative, avec un potentiel de corrosion passant de –28,7 à –306,9 mV et une densité de courant de corrosion augmentant de 7,76 nA à 3,97 µA. Cette détérioration est attribuée à des films passifs instables et à des discontinuités microstructurales causées par une saturation hétérogène en azote. En revanche, l'AISI 316L a présenté un comportement de corrosion amélioré : malgré une augmentation de la densité de courant de 10,5 nA à 6,69 µA, la spectroscopie d'impédance a confirmé une forte réponse capacitive, indiquant la formation d'une couche γN plus stable et homogène. La présence de molybdène dans le 316L a joué un rôle clé dans le renforcement de la stabilité du film passif. Ces résultats indiquent que la nitruration plasma a amélioré la dureté dans les deux alliages par renforcement par l'azote interstitiel, mais a affecté la corrosion différemment selon la composition de l'alliage : dégradation dans le 304 due à l'instabilité du film passif, et renforcement dans le 316L grâce à l'effet stabilisant du molybdène.

Mots-clés : Aciers inoxydables ; AISI 316L ; AISI 304 ; Dureté ; Corrosion ; Nitruration par plasma.

الملخص

الهدف من هذه الدراسة هو تطبيق عملية النتردة بالبلازما عند درجة حرارة منخفضة على أنواع الفولاذ المقاوم للصدأ لتقييم تأثيرها على الخصائص الهيكلية والميكانيكية والكهربائية الكيميائية. أظهرت تحاليل حيود الأشعة السينية عن تكوين الأوستنيت المتمدّد المسؤول عن تحسين الصلادة. حيث انخفض عمق الاختراق في اختبار النانو انطباع من ~1150 إلى 1100 نانومتر في 304 ومن ~1100 إلى 1070 ملي نيوتن في 316 و ذلك تحت حمل 100 نانومتر.

أما من الناحية الكهروكيميائية، فقد أظهر الفولاذ 304 تراجعًا واضحًا في مقاومة التآكل (انتقال جهد التآكل من –28.7 إلى –306.9 ميلي فولت وارتفاع كثافة التيار من 7.76 نانو أمبير إلى 3.97 ميكرو أمبير)، ويُعزى ذلك إلى تكون طبقات غير مستقرة وانقطاعات مجهرية في الغشاء الواقي نتيجة تشبع غير متجانس بالنيتروجين.

في المقابل، أظهر الفولاذ 316 تحسنًا في السلوك التآكلي، إذ حافظ على استجابة سعوية في مطياقية الممانعة الكهروكيميائية رغم زيادة التيار من 10.5 نانو أمبير إلى 6.69 ميكرو أمبير، مما يدل على تكوين طبقة أوستنيت متمدّد أكثر تجانسًا واستقرارًا بفضل وجود الموليبدينوم، الذي عزز ثبات الطبقة السلبية.
تُفسَّر هذه النتائج بأن النترنة حسّنت الصلادة في كلا السبيكتين بفضل إدخال ذرات النيتروجين بين مواقع الشبكة البلورية (تقوية محلول صلب)، غير أن السلوك التآكلي ارتبط بالتركيب الكيميائي: حيث أدى غياب الموليبدينوم في 304 إلى فقدان الحماية السطحية، بينما سمح وجوده في 316 Lبالحفاظ على مقاومة التآكل.

الكلمات المفتاحية: الفولاذ المقاوم للصدأ ; AISI 316L ; AISI 304 ; الصلادة ; التآكل ; النتردة بالبلازما.

List of Symbols and Abbreviations

Symbol / Abbreviation	Meaning / Notes
CDTA	Centre de Développement des Technologies Avancées
AISI	American Iron and Steel Institute (steel grade designation)
SS	Stainless steel
304, 304L	AISI 304, 304L austenitic stainless steel grades
316L	AISI 316L austenitic stainless steel (low carbon, contains Mo)
CrN, Cr_2 N	Chromium nitride phases
Cr, Ni, Mo, C, N	Chromium, Nickel, Molybdenum, Carbon, Nitrogen (elements)
N_2 , H_2 ,NH3	Molecular nitrogen, molecular hydrogen (process gases), Ammonia gas
γ (gamma)	Austenite phase (γ-Fe, FCC structure)
γN / S-phase	Expanded austenite (nitrogen supersaturated metastable austenite)
Fe_4 N, Fe_2 $_{-3}$ N	Iron nitride phases
ε, γ′, α	Other possible phases (ε-phase, γ′, α-phase)
XRD	X-Ray Diffraction
OM	Optical Microscopy
Nanoindentation / Oliver-Pharr	Instrumented indentation technique / analysis method
2θ	Diffraction angle (degrees) in XRD patterns
d	Interplanar spacing (Å or nm)
λ	X-ray wavelength (e.g., Cu Kα ≈ 1.5406 Å)
Bragg's law	$n\lambda = 2 d \sin\theta$ (relationship used in XRD)
ICDD / JCPDS / PDF card	Standard diffraction reference (e.g., PDF card No. 31-0619 for 316L)
SEM	Scanning Electron Microscopy
PVD	Physical Vapor Deposition (mentioned in coatings context)
S	Contact stiffness (dF/dh) during nanoindentation
dF/dh	Slope of unloading curve (load vs. displacement)
A_c (or Ac)	Projected contact area between indenter and specimen

E_r	Reduced elastic modulus
E_i	Elastic modulus of the indenter (diamond)
E	Young's modulus of the specimen
ν, ν_i	Poisson's ratio of the specimen (ν) and indenter (νi)
Hardness (H)	Hardness value (e.g., GPa, HV)
HV	Vickers Hardness number
GPa, MPa, Pa	Units of stress/modulus
nm, µm, mm	Length units: nanometer, micrometer, millimeter
mN, N	Force units: millinewton, newton
Tafel	Potentiodynamic polarization technique
E_corr (Ecorr)	Corrosion potential (mV vs reference electrode)
I_corr (Icorr)	Corrosion current density ($A \cdot cm^{-2}$; reported in nA or µA)
β_a, β_c	Anodic (βa) and cathodic (βc) Tafel slopes (mV/decade)
R_ct	Charge transfer resistance ($\Omega \cdot cm^2$)
R_p	Polarization resistance ($\Omega \cdot cm^2$)
EIS	Electrochemical Impedance Spectroscopy
Nyquist plot	Plot of real (Z') vs imaginary (Z'') impedance
Bode plot	Magnitude and phase vs frequency plot (EIS)
C_dl	Double layer capacitance ($F \cdot cm^{-2}$)
Z	Impedance (complex quantity)
kPa, mbar	Pressure units: kilopascal, millibar
% (e.g., 80% N_2 –20% H_2)	Gas composition percentages
T	Temperature (°C or K)
t	Time (h, min) — nitriding duration
n	Integer order in Bragg's law (usually n = 1)
σ	Stress (Pa)
ε (strain)	Strain (dimensionless, not phase ε)
w%	Weight percent (composition units)
Ref. electrode	Reference electrode (e.g., Ag/AgCl, SCE)

Table of Contents

List of Figures

List of Tables

Presentation of CDTA

The Centre for the Development of Advanced Technologies (CDTA) is a public scientific and technological institution (EPST). Its mission is to carry out scientific research, technological innovation, valorization, and training activities in various fields, notably information sciences and technologies, industrial technologies and robotics, material deposition and treatment, as well as laser applications and technologies.

Through these missions, the CDTA plays an essential role in the development of knowledge and its transformation into know-how and products necessary for economic and social progress. The CDTA possesses expertise and know-how accumulated over more than thirty years of activity, which gives it national recognition. Aware of this strength, the Center's management strives to maximize cross-disciplinary collaboration in order to further specialize in integrative technologies, aiming for technological development capable of improving citizens' daily lives. Thus, six impact areas have been targeted by the current scientific and technological roadmap of the Center:

- Health
- Energy
- Environment
- Water
- Digital technologies
- Industrial technologies

History of CDTA

- **1982**: Creation of the *Centre for the Development of Advanced Techniques* within the *Commission for New Energies (CEN).*
- **March 22, 1988**: Creation of the *Centre for the Development of Advanced Technologies (CDTA)* by Presidential Decree No. 88-61.
- **November 29, 1988**: Internal organization of CDTA established by Interministerial Order.
- **December 28, 1988**: Attachment of the *Silicon Technology Development Unit* to CDTA by Ministerial Order.
- **November 16, 1999**: Executive Decree No. 99-256 defining the modalities of creation, organization, and functioning of public scientific and technological establishments.

- **December 1, 2003**: Executive Decree No. 03-457 amending and supplementing Decree No. 88-61 of March 22, 1988, establishing the CDTA and granting it the status of a *Public Scientific and Technological Establishment (EPST)*.
- **September 2, 2006**: Interministerial Order establishing the internal organization of CDTA with the following research divisions:
    - Systems Architecture and Multimedia
    - Microelectronics and Nanotechnology
    - Ionized Media and Laser
    - Production Engineering and Robotics
- **November 8, 2007**: Interministerial Order supplementing the Interministerial Order of September 2, 2006, concerning the activities of the *Silicon Technology Development Unit*.
- **March 5, 2011**: Ministerial Order No. 143 establishing a *Photonics and Optics Research Unit* in Sétif, attached to CDTA.
- **August 21, 2012**: Executive Decree No. 12-316 (3 Chaoual 1433) creating the *Research Center in Semiconductor Technology for Energy (CRTSE)*.
- **January 4, 2014**: Order No. 003 creating a *Research Unit for Optoelectronic Components and Devices*.

General Introduction

General Introduction

Engineering materials are the core of industrial and technical development. Their unique properties determine the efficiency and lifespan of many vital systems and components. Stainless steel holds an advanced position among these materials, notably due to its exceptional corrosion resistance, formability, and high durability. However, the increasing use of these alloys in harsher environments such as aggressive chemical media and conditions requiring high resistance to both corrosion and wear has pushed researchers to seek strategies for enhancing their surface properties without compromising their bulk characteristics.

Among advanced surface treatment technologies, Plasma Nitriding emerges as an effective solution for improving the surface hardness and corrosion resistance of stainless steel. This process aims to integrate nitrogen atoms into the metal's outer surface at precisely controlled temperatures, leading to the formation of a hard, nitride-rich layer called the S-layer. In this context, this work focuses on studying the effect of low-temperature plasma nitriding on the properties of two of the most widely used austenitic stainless steel types: Stainless Steel 304 and Stainless Steel 316L. A strict treatment temperature not exceeding 400 c° was chosen specifically to avoid the precipitation of chromium nitrides (CrN) along grain boundaries, a phenomenon that can lead to "sensitization" of the stainless steel and drastically reduce its corrosion resistance.

The objectives of this thesis are to study and analyse the morphological and phase changes that occur on the surface of 304 and 316L steels after the plasma nitriding process. This is done by evaluating the surface mechanical properties, especially hardness, to determine the process's effectiveness in enhancing wear resistance, and by determining the electrochemical corrosion resistance of the treated specimens compared to the original, untreated specimens in a specific corrosive environment.

To achieve these objectives, the thesis is organized into the following chapters:

Chapter 1: Bibliographic Review

This chapter addresses the concept of Nitriding and its various types, with a particular focus on the Plasma Nitriding technique. It also includes a review of previous works and experiments conducted on stainless steel, summarizing their findings regarding the formation of a protective layer and the enhancement of corrosion resistance.

Chapter 2: Stainless Steel Alloys

This chapter is dedicated to describing the Stainless Steel 304 and 316L alloys. Their chemical composition, crystal structure (austenite), and fundamental mechanical and physicochemical properties will be detailed to provide a comprehensive overview of both.

Chapter 3: Experimental and Characterization Techniques

This chapter describes in detail the methodology followed in the study, starting from the specimen preparation method, through the Plasma Nitriding unit and operating conditions (temperature, pressure, gas composition), up to the approved testing and characterization techniques: X-ray Diffraction (XRD), Nanoindentation, Tafel polarization test, Electrochemical Impedance Spectroscopy (EIS), and Optical Microscope.

Chapter 4: Results and Discussion

In this final chapter, the experimental results obtained after the treatment will be presented and discussed. The properties before and after nitriding will be compared, and an analysis of the noticeable improvements in mechanical properties and corrosion resistance will be provided, which yielded satisfactory and clear results.

The findings of this research contribute to deepening our understanding of the effect of low-temperature plasma nitriding as an effective solution for increasing the surface performance of stainless steel, thus opening up new prospects for its applications in high-demand industries.

Chapter 1

Bibliographic Review

Chapter 1: Bibliographic Review

1.1. Nitriding

Nitriding is a tribological engineering process that modifies surface properties to enhance mechanical performance, specifically hardness, wear resistance, and corrosion resistance of steel.

This process focuses on saturating the steel surface with nitrogen. It is carried out in a gaseous ammonia (NH_3) atmosphere at temperatures ranging from 480 to 650 °C. At this temperature, ammonia almost completely dissociates according to the reaction $2NH_3 \rightarrow 2N + 3H_2$. The released nitrogen then diffuses into the metal (alpha iron), gradually saturating its surface. After nitriding, the metal is cooled down to approximately 200 °C in an ammonia flow. The nitriding process can be performed using various methods [1.1].

1.1.1. Nitriding processes

The most commonly used nitriding processes include salt bath nitriding, gas nitriding, and ion nitriding (also known as low-pressure nitriding). Among these methods, ion nitriding is the most recent. Although it requires a significant investment in equipment, it offers several advantages over the other techniques, such as lower treatment temperatures and shorter processing times [1.2].

1.1.1.1. Salt bath nitriding

Salt bath nitriding involves the use of a molten salt that contains a nitrogen source. When heated, the salt releases nitrogen, which diffuses into the surface of the steel once the part is immersed and heated to the salt's fusion temperature. This process typically occurs at temperatures between 500 and 550 °C. It allows for the formation of relatively thick compound layers, although the diffusion layer is often limited in thickness [1.3].

1.1.1.2. Gas nitriding

Gas nitriding is typically carried out in a bell-type or pit furnace equipped with a forced convection system to ensure proper gas circulation. The basic principle involves introducing gaseous ammonia into the furnace, where controlled stirring and temperature regulation facilitate the transfer of nitrogen atoms from the ammonia to the surface of the material. At

temperatures around 600 °C, a 10-hour treatment can produce a compound layer up to 20 microns thick, and under certain conditions, the diffusion layer can exceed 150 microns [1.4].

1.1.1.3. Plasma ion nitriding

During plasma ion nitriding, the parts are placed in a vacuum chamber within an electric field that ionizes nitrogen. The electric field is established between the chamber wall, acting as the anode (+), and the parts positioned as the cathode (-). Nitrogen is introduced under vacuum until a pressure of about 1 mbar is reached. Nitrogen ionizes in the immediate vicinity of the cathode, i.e., the parts. The positively charged nitrogen ions accelerate with high energy toward the negatively charged cathode. During this ion bombardment, the passivated surface is atomically sputtered (cathodic sputtering) and ideally activated.

Nitrogen then penetrates the surface and forms a superficial layer on the treated parts. Simultaneously, the kinetic energy of the nitrogen ions causes a temperature increases at the surface being bombarded, reaching the actual nitriding temperature. Generally, no external heat source is required for this nitriding process.

The typical nitriding temperature for stainless steels ranges between 550 and 580 °C, though it can be lower or higher depending on various factors. The ion nitriding duration varies from 10 to 24 hours depending on the desired case depth. Surface hardness increases to between 950 HV and 1100 HV, with a hardened layer depth of approximately 0.1 to 0.2 mm [1.5].

1.1.2. Applications of nitriding

Nitriding is a long-established thermochemical treatment, with industrial applications dating back to the 1950s. It is primarily known for its ability to harden the surface of fully machined mechanical parts by significantly improving [1.6]:

- **Surface hardness of steels**: this increases their wear resistance, especially in mechanical parts subjected to friction and high loads, such as gears, camshafts, and pistons [1.7].
- **Wear resistance**: by creating thin and hard nitrided layers, nitriding protects components from abrasive and adhesive wear, thereby extending the service life of industrial part [1.8].
- **Corrosion resistance**: Certain nitrided layers, particularly on stainless steels, enhance corrosion resistance, especially in aggressive environments [1.9].
- **Reduction of thermal and mechanical fatigue**: By improving surface properties, nitriding increases fatigue resistance in parts subjected to cyclic loads useful in aerospace and automotive applications [1.10].

1.1.3. Specific industrial applications

- Automotive components (camshafts, cylinder heads).
- Cutting tools and dies.
- Aerospace components.
- Agricultural machinery parts [1.11].

1.2. Niriding of austenitic stainless steel

Austenitic stainless iron (such as 316L and 304) has a Face-Centered Cubic (FCC) crystal structure, which gives it the mechanical and chemical properties that make it resistant to corrosion and rust. But as we mentioned previously, when this type of iron is exposed to the nitriding process, nitrogen atoms intervene in the crystal lattice and cause important changes in the structural composition and properties [1.12].

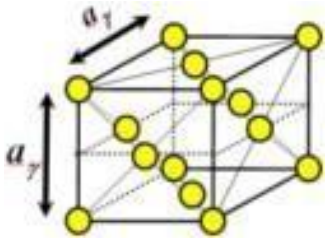

Figure 1.1. Face-Centered Cubic (FCC) crystal structure [1.12]

The nitriding mechanism begins with nitrogen atoms penetrating the surface and penetrating between atoms in the crystal lattice, where the nitrogen atoms settle at interstitial sites within the FCC lattice. This increases the hardness, as the presence of nitrogen atoms in these interfacial sites leads to internal tension within the crystal lattice, which causes local expansion in the lattice and increases the surface hardness [1.12].

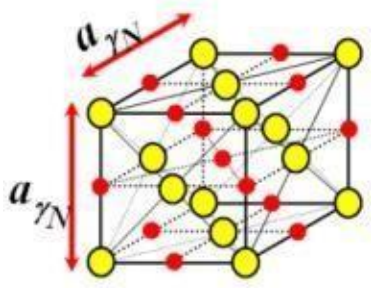

Figure 1.2. Face-Centered cubic (FCC) crystal structure after nitrogen treatment [1.12]

The tension create by the nitrogen atoms reduce the sliding within the crystal lattice, which increases resistance to deformation (increased hardness). This phenomenon is known as interstitial solid solution strengthening,

and it is one of the main mechanisms that improve the mechanical properties of nitride stainless steel [1.13].

1.3. Effect of nitriding on the microstructure of stainless steel

Plasma nitriding presents one of the few viable methods for enhancing the surface hardness of these steels [1.14] and these improvements are partly due to the layer that forms on the surface after the treatment. This is a diffusion layer in which nitrogen has diffused interstitially. This can be confirmed by observing it using Optical Microscopy (OM), In Figure 1.3, the cross-sectional views reveal an expanded austenite layer at the surface of the specimen [1.15].

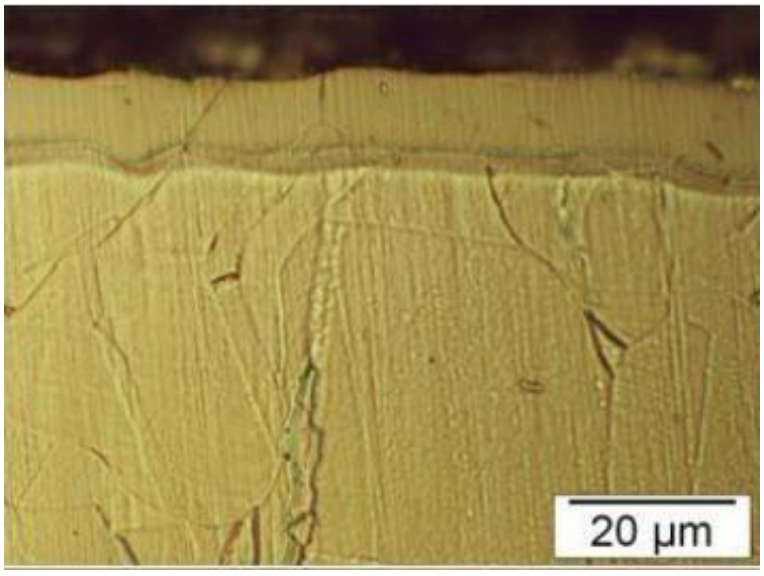

Figure 1.3. Transverse micrographic sections observed under the microscope [1.15]

A study published by T. Thirie et al. [1.15] where he treated a stainless steel for 4 hours at 420°C in 90%N_2-10%H_2(b), showing diffraction peaks associated with the nitrided layer as well as diffraction peaks of the austenite substrate. Figure 1.4-A shows an X-ray diffraction diagram of an untreated specimen and Figure 1.4-B shows a diffraction diagram of a treated specimen. Each stainless steel diffraction peak (ɣN) is associated, at the smallest angles, with an austenite diffraction peak in the austenite phase (ɣN). Expanded austenite is a metastable phase saturated with nitrogen which is expanded: it is called a solid solution of disordered and distorted cubic nitrogen [1.15].

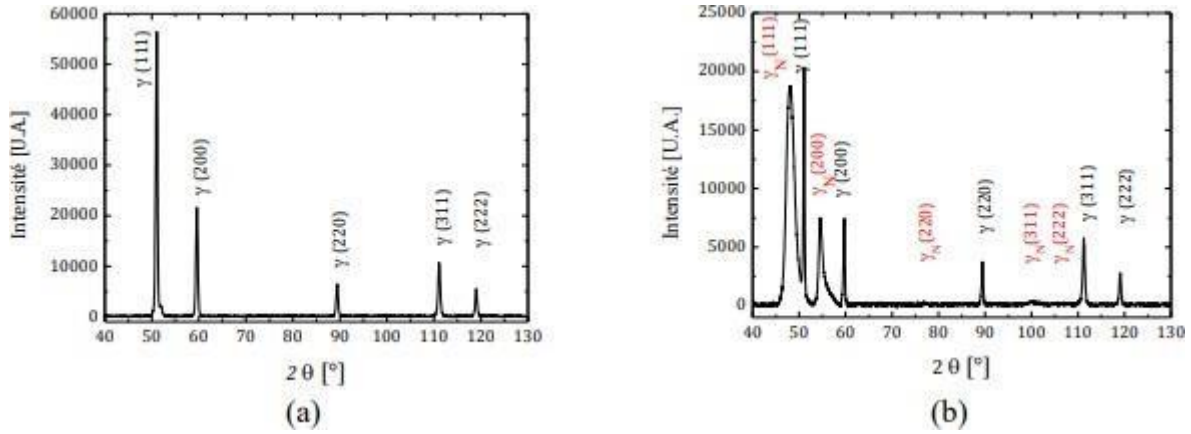

Figure 1.4. X-ray diffractograms in the θ-2θ (CoKα) configuration of a non-nitrurated austenitic stainless steel specimen (a) and after 4 h nitriding at 420°C in 90% N_2-10% H_2 (b) [1.15]

1.3.1. Effect of time process forming the nitrogen layer

we noticed that it is important that the treatment time plays an important role in the deposition of the nitrogen layer, and this is evident in the following image after we treated the specimens corresponding to the kinetics of 420°C in a mixture of 90% N_2-10% H_2 over a varied period of time and then saw the development of the deposited layer using a cross-sectional optical microscope [1.15].

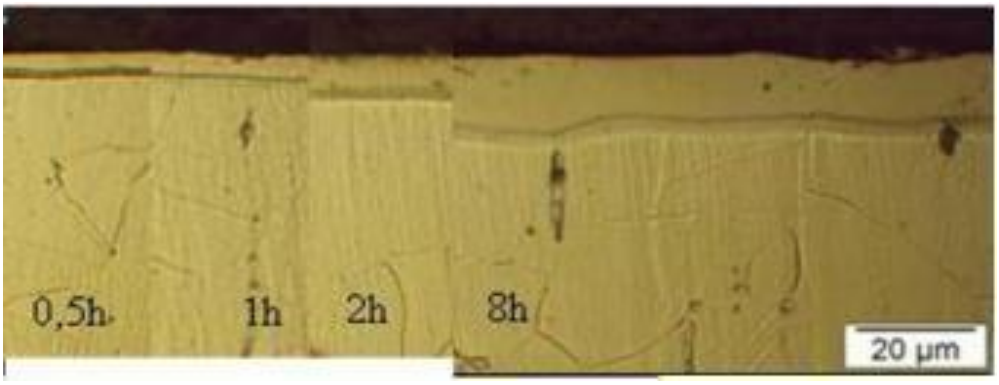

Figure 1.5. Cross-sectional optical micrographs of 316L specimens nitraded at 420°C in a 90% N_2-10% H_2 mixture without prior stripping step in the diode reactor [1.15]

1.3.2. Effect of temperature process on the microstructure

A study entitled "Structural Characterization of Ion Nitrided 316L Austenitic Stainless Steel" was conducted by O. Gokcekaya et al. In this work, AISI 316L plasma nitrided was carried out in a gas mixture of 80% nitrogen (N_2) and 20% hydrogen (H_2), at a total pressure of 1 kPa. The nitriding treatments were performed at temperatures of 450°C, 500°C, and 550°C, with durations of 2 hours, 4 hours, and 9 hours. The structural characterization was based on several assessments, including [1.16]:

- The evaluation of phase distribution through Rietveld analysis of X-ray diffraction (XRD) patterns along with peak fitting procedures;
- The hardness profile and nitride layer thickness, evaluated using microhardness testing and microscopic measurements.

Figure 1.6 presents the XRD patterns of the nitride layers formed on AISI 316L specimens treated at various nitriding temperatures and durations. The primary and secondary phases identified across all patterns include γ, γN, γ′, α, ε, CrN, and/or Cr_2 N." Figure 1.6. The formation of the γN phase, resulting from nitrogen diffusion into the γ matrix, that was detected from the peaks formed by shifting the peaks of the matrix γ phase to a smaller diffraction angle [1.17] which is essential as it significantly contributes to achieving both high surface hardness and excellent corrosion resistance [1.16]. We can conclude that as the temperature increased, the amount of the ε and γN phases showed a continuous decrease, while those of the α and CrN phases showed an increase. On the other hand, the amount of γ′ and γ phases remained almost constantAfter 4 hours, Cr_2 N becomes evident, especially at 500 °C [1.16]. At 9 hours, all phases appear, but at 550 °C, γ and ε sharply decline, and CrN and Cr_2 N become dominant. Generally, increasing the temperature up to 500 °C enhances nitrogen diffusion and γN formation. However, at 550 °C, denitriding occurs, leading to the decomposition of γN into CrN and α or Cr_2 N and α, depleting chromium and reducing corrosion resistance [1.16]. The γ′ phase appears to result from γN transformation at high nitrogen content but remains stable across conditions. The nitrided layer consists of a diffusion layer (γN, CrN, Cr_2 N, α) and a compound layer (ε, γ′). The ε-rich compound layer, observed at 450–500 °C, is hard but brittle. At 550 °C, ε decreases significantly due to denitriding, with a corresponding increase in CrN and Cr_2 N precipitates. Hardness variation is thus mainly linked to changes in γN, ε, and α phases and the formation of chromium nitrides [1.16].

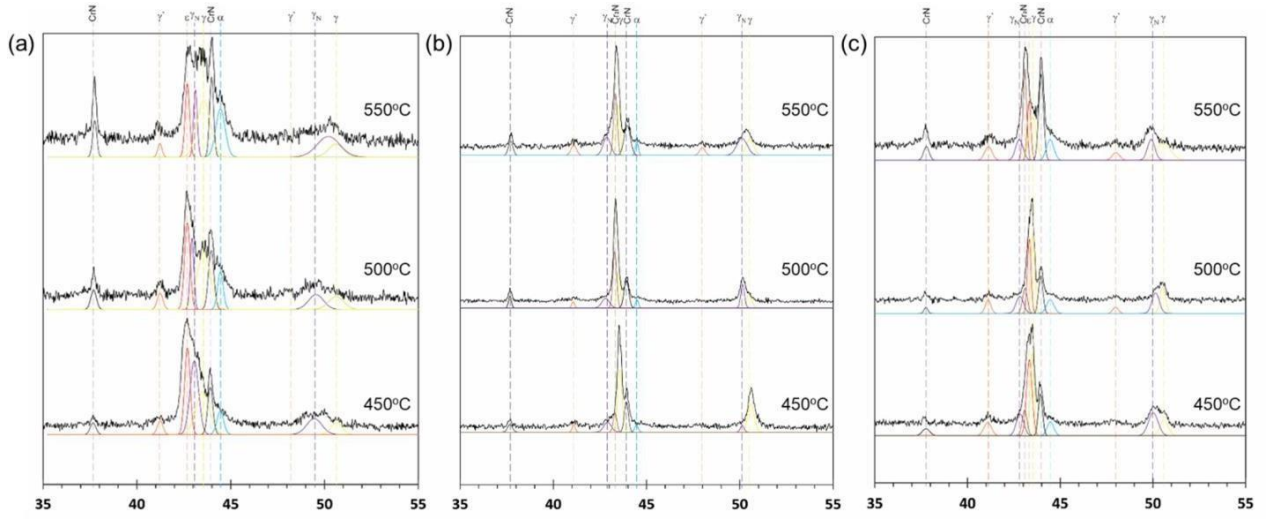

Figure 1.6. XRD pattern of the nitride layer on 316L specimes at various temperatures for (a) 2 h, (b) 4 h, and (c) 9 h [1.16]

Optical microscopy (OM) images of the nitrided cross-sections revealed the nitride layer as a darker region, indicating nitrogen diffusion and the associated phase transformations (Figure 1.7 a–c). Some delamination of the outer nitride layer was observed, likely due to the formation of the brittle ε phase, as shown in Figure 1.7 a (iii). The nitride layer thickness was clearly visible in the OM images (Figure 1.7), aligning well with the microhardness measurement results. Based on the hardness-depth profiles and OM observations, the estimated nitride layer thicknesses under different nitriding conditions were approximately 15 µm at 450 °C, 40 µm at 500 °C, and 45 µm at 550 °C [1.16].

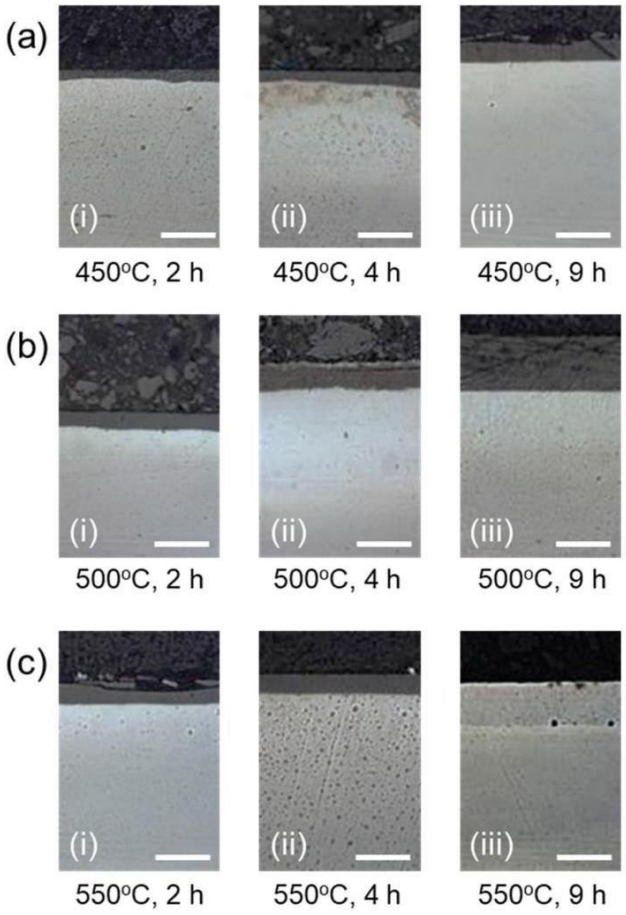

Figure 1.7. OM images of the nitride layer of 316L specimens for (a–c) various nitriding time and temperature [1.16]

1.4. Effect of nitriding on the mechanical properties of stainless steels

Throw the study entitled "Structural Characterization of Ion Nitrided 316L Austenitic Stainless Steel" was conducted by O. Gokcekaya et al. It was surveyed that after 2 hours of nitriding, the surface hardness increased significantly from approximately 900 HV to 2000 HV as the temperature rose from 450°C to 500°C. However, a further increase in temperature to 550°C led to a decrease in hardness to around 1300 HV. A similar trend was observed after 4 hours of nitriding, with hardness increasing from about 900 HV to 1900 HV between 450 °C and 500 °C, followed by a decline to roughly 1400 HV at 550 °C.

Interestingly, the 9-hour nitriding treatment exhibited a different pattern: the surface hardness decreased from 2100 HV at 450 °C to 1500 HV at 500 °C, and further declined to 1400 HV at 550 °C [1.16].

Another study entitled "Nanoindentation Study of Hardness and Modulus Changes in Nitrided Stainless Steel." X. Li et al. aims to study the effect of the nitrification process on the mechanical properties of stainless steel using nanoindentation testing (testing using a microscope to press the surface of the material precisely at the nanoscale). Emphasis was

placed on the effect of nitrification on the hardness and elastic modulus of stainless steel (AISI 304) after applying nitrification processes under different conditions. was carried out at 570 °C for 4, 8, and 12 hours. The nanoindentation device was used to measure the hardness and elastic modulus at a depth of several micrometers below the surface, so that it was observed that the hardness and elastic modulus increase significantly near the surface, and the results obtained are in Table 1.1 below [1.18].

Nitriding Condition	**Hardness (GPa)**	**Elastic Modulus (GPa)**
Unnitrided (Base material)	2.1	180
Nitriding: 4 hours, 570°C	2.5	185
Nitriding: 8 hours, 570°C	2.9	190
Nitriding: 12 hours, 570°C	3.1	195

Table 1.1. Results of Nanoindentation on Nitrided AISI 304 Stainless Steel [1.18]

Through the experiment and the results obtained after inserting the specimens to examine the hardness, it was found that the nitriding process is effective in increasing the hardness of the surface, but we have confirmed that the curing time has an important role in increasing the hardness, and this is perhaps due to the layer formed after curing.

1.5. Conclusion

Additionally, if austenitic stainless steels, such as AISI 316L, are treated at the temperatures used in conventional nitriding treatments of steels (typically about 550°C), they can suffer a significant decrease in their corrosion resistance due to the formation of chromium nitride CrN, precipitation with the expense of chromium in their solid solution, which would otherwise be used in the construction the protective film on their surfaces [1.19].

But when performed at lower temperatures around 400 °C, this process results in the formation of a supersaturated interstitial austenite layer, known as the S-phase. This layer is characterized by high hardness, excellent wear resistance, and good corrosion resistance, although it typically exhibits limited thickness [1.20]. At temperatures exceeding 450°C, a multiphase “dark” layer forms, consisting of iron and chromium nitride precipitates. While this layer offers increased hardness, it may partially compromise the steel’s corrosion resistance and alter its corrosion mechanism [1.20]. Nonetheless, such hard layers are frequently utilized as intermediate coatings for thin, ultra-hard films deposited using Physical Vapor Deposition (PVD) techniques [1.21].

References

[1.1] Poloukhine, P., Grinberg, B., Kantenik, S., Jadan, V., & Vassiliev, D. (1967). *Technologie des métaux* (V. Polonski, Trad.). Moscou : Éditions Mir.

[1.2] Mohamed Mounès ALIM, « Réalisation et caractérisation d'un réacteur plasma hybride - Application : traitement de surface par nitruration ». Thèse de doctorat (2017). USTHB, Algérie.

[1.3] B. Grellet, Journées Spécialisées du CACEMI, Paris, Mars (1999).

[1.4] C. Dermaix, G. Veyssiere, L. Henry, Journées Traitements de Surface Anti- Corrosion, Limoges,Novembre (2000).

[1.5] David, S., & Ordenbach, H. (1999). *Les aciers inoxydables : Propriétés, mise en œuvre, emploi, normes*. Paris : Tec & Doc / Lavoisier.

[1.6] Barrallier, L. (1989). "Modélisation des contraintes résiduelles dans les couches nitrurées." PhD Thesis, University of Paris XIII, France.

[1.7] Totten, G. E. (2006). Steel Heat Treatment: Metallurgy and Technologies. CRC Press.

[1.8] Blawert, C., et al. (2006). "Nitriding of steels — a review." Surface and Coatings Technology, 201(10), 4917–4923.

[1.9] Lin, H., & Bell, T. (1996). "Surface properties of plasma nitrided stainless steel." Surface and Coatings Technology, 81(2–3), 219–227.

[1.10] Assadi, H., et al. (2003). "Nitriding of steels: A review of recent developments." Surface Engineering, 19(4), 283–291.

[1.11] ASM International Handbook, Volume 4A: Steel Heat Treating Fundamentals and Processes, 1991.

[1.12] Michler, T. Austenitic Stainless Steels. In Reference Module in Materials Science and Materials Engineering; Elsevier: Amsterdam, The Netherlands, 2016; ISBN 978-0-12-803581-8.

[1.13] Hull, D., & Bacon, D.J. (2011). Introduction to Dislocations. 5th Edition. Butterworth-Heinemann.

[1.14] Bekmurzayeva, A.; Duncanson, W.J.; Azevedo, H.S.; Kanayeva, D. Surface modification of stainless steel for biomedical applications: Revisiting a century-old material. Mater. Sci. Eng. C 2018, 93, 1073–1089.

[1.15] Zhang, Z.L.; Bell, T. Structure and corrosion resistance of plasma nitrided stainless steel. Surf. Eng. 1985, 1, 131–136.

[1.16]. Ozkan Gokcekaya, Celaletdin Ergun, Turgut Gulmez, Takayoshi Nakano, and Safak Yilmaz "Structural Characterization of Ion Nitrided 316L Austenitic Stainless Steel" 2022.

[1.17] Borgioli, F. From Austenitic stainless steel to expanded austenite-S phase: Formation, characteristics and properties of an elusive metastable phase. Metals 2020, 10, 187.

[1.18] Li, X., et al. (2017). "Nanoindentation Study of Hardness and Modulus Changes in Nitrided Stainless Steel".

[1.19] Tony Thiriet. Traitement mécaniques et thermochimiques couplés sur acier inoxydable et alliage base nickel austénitiques. Autre. Institut National Polytechnique de Lorraine, 2010. Français.

[1.20] http://journalmt.com/pdfs/mft/2019/05/04.pdf

[1.21] Petr Faltejsek, Zdeněk Joska, Zdeněk Pokorný, David Dobrocký, Zbyněk Studený "Effect of Nitriding on the Microstructure and Mechanical Properties of Stainless Steels"2019.

Chapter 2

Stainless Steel Alloys

Chapter 2: Stainless Steel Alloys

2.1. Introduction

Stainless steel is the most widely used material in most fields, including everyday life. Stainless steel helped solve the most significant problems threatening iron and steel industries: rust and corrosion. This chapter contains some information about stainless steel, including its types and grades, particularly its properties, it also includes a superficial comparison of the two grades' resistance to corrosion. Note that the properties listed in this section are specific to the grades under study, which are 304 and 316L.

2.2. Types of Stainless Steels

Many stainless steel grades additives allow changing physical and mechanical properties based on the environment the metal is expected to bear. Based on the exact structure, it can be classified in four main categories.

2.2.1. Austenitic Stainless Steels

Austenitic stainless steels contain between 16 and 25% of Cr and can also contain nitrogen in solution, both of which contribute to their relatively high corrosion resistance. The Face-Centered Cubic (FCC) crystal structure of austenitic stainless steels is achieved by sufficient additions of the austenite stabilizing elements like nickel, manganese and nitrogen [2.1] which make them non-magnetic in their annealed condition [2.2] and grants them high ductility and toughness. This structure allows substantial plastic deformation before fracture [2.3].

Austenitic stainless steels cannot be hardened by heat treatment but have some useful properties of retaining a useful level of ductility and toughness [2.1], and maintain good strength over a wide temperature range, making them suitable for both cryogenic applications like storage tanks for liquefied gases and high-temperature environments such as in heat exchangers [2.3]. Common Grades are 304, 316, 304L, 316L, 321.

2.2.2. Ferritic Stainless Steels

These stainless steels have a Body-Centered Cubic (BCC) crystal structure and are magnetic [2.4]. The Cr content in ferritic steels is between 13 and 30% and the C is less than 0.10%. As complementary alloying elements, it is preferable to add element that stabilize ferrite such as molybdenum to improve corrosion resistance. Carbon and nitrogen have a significant effect on corrosion resistance due to their low solubility in the ferritic matrix of these steels [2.5]. Ferritic steels must heat treated because the diffusion of alloying elements and C (and Cr) in ferrite at each temperature is 102 to 103 times faster than in austenite, and thermal activation processes [2.5]. Those stainless steels are called ferritic because they contain primarily ferritic microstructures at all temperatures and cannot be hardened through heat treatment and quenching [2.6]. They have relatively poor high-temperature strength. Ferritic steels are chosen for their resistance to stress corrosion cracking, which makes them attractive alternatives to austenitic stainless steels [2.6].

Common Grades are: 430, 409, 444.

2.2.3. Martensitic stainless steels

These stainless steels also have a BCC crystal structure and are magnetic. They are sometimes classified as low-carbon and high-carbon martensitic stainless steels. They contain 12 to 14% Cr, 0.2 to 1% molybdenum, and no significant amount of Ni [2.7]. They can be hardened by heat treatment (quenching and tempering), which significantly increases their strength and hardness [2.8, 2.9]. The working properties of chromium martensitic steels, which differ from all other stainless steel groups in their high hardness and heat treatment values, vary to a large extent.

Common Grades are: 410, 420, 440C.

2.2.4. Duplex Stainless Steels

These stainless steels have a mixed microstructure of austenite and ferrite, hence the name duplex. This combination gives them high strength and excellent corrosion resistance, often superior to austenitic stainless steels [2.10].

Common Grades are: 2205, 2507.

2.3. Stainless steel classes

2.3.1. The 200 Series (Austenitic - Manganese Austenitic)

These are austenitic stainless steels but with manganese instead of nickel. They are developed to reduce cost when nickel prices are high. Their properties are generally similar to 300 series stainless steels, but they may have slightly different corrosion resistance [2.2, 2.10].

2.3.2. The 300 Series (Austenitic)

The most widely used series of stainless steel. They are austenitic, non-magnetic in the annealed conditions, and known for their excellent corrosion resistance, good formability, and weldability. They contain significant amounts of chromium and nickel.

AISI 304 and 316 are the most common grades in this series. AISI 304 is also commonly known as 18/8 steel as it contains 18% chromium and 8% nickel [2.11].

2.3.3. The 400 Series (Austenitic)

Ferritic and martensitic alloys form this series of stainless steel. These grades are available for heat treatment. Providing a good combination of strength and high wear resistance. The corrosion resistance properties are lower than 300 series [2.4].

2.4. Chemical properties of stainless steels

Chemical properties are what make this material special and give it its uniqueness.

2.4.1. High oxidation resistance

This distinguishing property of stainless steel is responsible for its many unique applications in the industry. High oxidation resistance is a result of chromium in stainless steel. The percentage of chromium can go up to 26% in some grades.

Other metals may be protected with coatings and anti-corrosion paints but once it wears off, the corrosion begins. In the case of stainless steel, any removal of the natural coating of chromium oxide due to surface damage is followed by the formation of a new coat on the exposed surface that prevents corrosion deterioration.

2.4.2. Biologically inert

Stainless steel is biologically inert, making it a logical choice for medical equipment such as surgical tools, trauma screws and plates. This property also makes it an ideal metal for cutlery products and kitchen appliances.

2.4.3. Resistance to acids, bases and organic materials

Stainless steel is resistant to a wide range of compounds. It is resistant to acids, bases as well as organic compounds. The resistance to acids varies for different grades. Some grades can resist highly concentrated acids while others may only be resistant to low concentrations.

Similar non-reactivity is observed with basic compounds and organic compounds. This makes stainless steel a highly suitable material for use in chemical industries for storage, handling and other processes.

Stainless steel also resists moisture, salt, sulphur, carbon dioxide and chloride compounds with ease. This helps it survive in several harsh environments for a longer period than most other metals [2.11].

2.5. Stainless steel proprieties

Material properties are intensive properties, that means they are independent of the amount of mass and may vary from place to place within the system at any moment. The basis of materials science involves studying the structure of materials, and relating them to their properties (mechanical, electrical etc.). Once a materials scientist knows about this structure-property correlation, they can then go on to study the relative performance of a material in a given application. The major determinants of the structure of a material and thus of its properties are its constituent chemical elements and the way in which it has been processed into its final form [2.1].

In this chapter we will study the properties of grades 304 and Grade 316L.

Grade 304 is the standard 18/8 austenitic stainless; it is the most versatile and most widely used stainless steel, available in the widest range of products, forms and finishes. It has excellent forming and welding characteristics

Grade 304 can be severely deep drawn without intermediate annealing, which has made this grade dominant in the manufacture of drawn stainless parts such as sinks, hollow-ware and saucepans. For severe applications it is common to use special 304DDQ (Deep Drawing Quality) variants.

Grade 316L low carbon is the standard molybdenum-bearing austenitic grade, second stainless steel in importance to 304. The molybdenum gives 316 better overall corrosion resistant properties than Grade 304, particularly higher resistance to pitting and crevice corrosion in chloride environments. It is readily brake, or roll formed, welded, soldered and cut by both thermal and mechanical methods. The austenitic structure gives excellent toughness, even down to cryogenic temperatures.

2.5.1. Chemical composition of 316L and 304 stainless steel

The following table lists the chemical composition of stainless steel alloys, including 304 and 316L.

Stainless steel	C ≤	Mn ≤	P ≤	S ≤	Si ≤	Cr	Ni	Mo	N ≤
304	0.08	2.00	0.045	0.03	1.00	18.0-20.0	8.0-11.0	–	–
316L	0.03	2.00	0.045	0.03	1.00	16.0-18.0	10.0-14.0	2.00-3.00	–

Table 2.1. Stainless steel chemical composition percentage (%) [2.12]

2.5.2. Physical properties

304 and 316L stainless steels physical properties are listed in the Table 2.1. below:

Grade	Density (kg/m^3)	Elastic Module (GPa)	Mean Coefficient of Thermal Expansion			Thermal Conductivity		Specific Heat 0-100°C (J/kg.K)	Electrical Resistivity (nΩ.m)
			0-100°C (µm/m/°C)	0-315°C (µm/m/°C)	0-538°C (µm/m/°C)	At 100°C (W/m.K)	At 500°C (W/m.K)		
304	7900	193	17.2	17.8	18.4	16.3	21.5	500	720
316L	8000	193	15.9	16.2	17.5	16.3	21.5	500	740

Table 2.2. Physical properties of 304 and 316L stainless steels [2.13, 2.14]

2.5.3. Mechanical properties

316L stainless steel has mechanical properties similar to 316, including tensile strength and elongation. However, it has a slightly lower yield strength, around 25 ksi, due to its lower carbon content.

304 stainless steel generally has lower tensile and yield strengths compared to 316. Its hardness profile also differs, making it less robust in certain demanding applications [2.7]. 304 and 316L stainless steel mechanical properties are listed in the Table 2.3. below:

Grade	Tensile Strength (MPa)	Yield Strength 0.2% Proof (MPa)	Elongation (% in 50mm)	Hardness	
				Rockwell B (HRB)	Brinell (HB)
304	515	205	40	92	201
316L	485	170	40	95	217

Table 2.3. Mechanical properties of 304 and 316L stainless steel [2.13, 2.14]

2.6. Corosion resistance

The 316 stainless steel is more resistant to intergranular corrosion than 304 stainless steel. Intergranular corrosion occurs along the grain boundaries of a material and can weaken its structural integrity. This is particularly important in applications where the material will be

exposed to high temperatures, such as in welding or heat treatment processes. The higher molybdenum content in 316 stainless steel helps prevent intergranular corrosion, which gives it good corrosion resistance in most environments, but the 304 stainless steel is not completely immune to corrosion. It can still be susceptible to corrosion in certain aggressive environments, such as those containing chlorides or acids [2.15].

316 stainless steel, also known as marine grade stainless steel. The addition of molybdenum enhances its corrosion resistance, making it suitable for use in harsh environments, including marine and chemical applications and helps it resist pitting and crevice corrosion, which are common forms of corrosion in chloride-rich environments. It is more resistant to corrosion in both acidic and alkaline environments. This makes 316 stainless steel a preferred choice for applications where it will be exposed to corrosive substances or environments [2.15].

Another important factor to consider when comparing the corrosion resistance of 304 and 316 stainless steel is their resistance to SCC. SCC is a type of corrosion that occurs under tensile stress in the presence of a corrosive environment. It can lead to sudden and catastrophic failure of the material. While both 304 and 316 stainless steel are resistant to SCC, 316 stainless steel has better resistance due to its higher molybdenum content [2.15].

2.7. Conclusion

We can say as conclusion that stainless steel is a remarkable material that combines a range of essential properties, making it one of the most important metals used in industries worldwide. Its diverse applications across industries highlight its versatility and durability. Despite its higher cost compared to other materials, the long-term benefits of stainless steel, such as reduced maintenance and extended lifespan, make it an indispensable choice for projects requiring high performance and sustainability.

References

[2.1] https://material-properties.org/what-is-austenitic-stainless-steel-definition/

[2.2] Stainless Steels, George E. Totten, Steven R. Callister, ASM International.

[2.3] https://dawangmetals.com/resources/austenitic-stainless-steel/

[2.4] Woldman's Engineering Alloys, George E. Totten, Steven R. Callister, ASM International.

[2.5] Les acier inoxydable.

[2.6] https://material-properties.org/what-is-ferritic-stainless-steel-definition/

|2.7] https://shop.machinemfg.com/316-stainless-steel-properties-everything-you-need-to-know/

[2.8] ASM Handbook, Volume 4: Heat Treating.

[2.9] Steel Metallurgy, A.K. Sinha.

[2.10] Duplex Stainless Steels, James M. Krolikowski, Michael W. Shultz, ASM International.

[2.11] https://fractory.com/what-is-stainless-steel/

[2.12] https://www.theworldmaterial.com/stainless-steel-chemical-composition/

[2.13] https://atlassteels.com.au/wp-content/uploads/2021/06/Stainless-Steel-304-304L-304H-Grade-Data-Sheet-23-04-21.pdf

[2.14] https://atlassteels.com.au/wp-content/uploads/2021/06/Stainless-Steel-316-316L-316H-Grade-Data-Sheet-27-04-21.pdf

[2.15] https://azure-b.com/blog/304-vs-316-stainless-steel-comparing-corrosion-resistance.html

Chapter 3

Experimental and Characterization Techniques

Chapter 3: Experimental and Characterization Techniques

3.1. Introduction

The aim of this chapter is to describe the experimental procedure carried out in the study. This includes the presentation of the experimental materials and equipment for the nitriding treatment of the stainless steel, as well as for the characterization of the nitrided surfaces.

The first section of the chapter will talk about the materials used for the preparation of the specimens . Two grades of stainless steel are used: AISI 304 and AISI 316L, then in the second section presents the materials and the equipment used for nitriding process. The nitriding treatment is carried out at various temperatures and durations in a homogeneous and synchronized manner, in conjunction with the annealing process. After nitriding process and to characterize the microstructural aspect of the nitrided surface, metallographic observations were carried out using OM, these observations allowed for the evaluation of grain morphology and size, as well as the detection of any nitrided layers formed on the surface of the specimens. Further structural analysis of the treated steels was performed using XRD, providing insight into phase composition and crystallographic changes resulting from the nitriding process. Finally, the mechanical properties of the specimens were evaluated using nanoindentation test.

3.2. Specimens Preparation

The specimens used in this study are made from austenitic stainless steel of grades 304 and 316L, provided in the form of plates. These materials were supplied by the CDTA.

3.2.1. Cutting and identification of the specimens

Once the raw material is received, it is necessary to cut it into smaller specimens with specific shapes and dimensions, compatible with the specimens holder dimensions of the nitriding system that will be used in the process. The cut specimens are given in Figure 3.1.

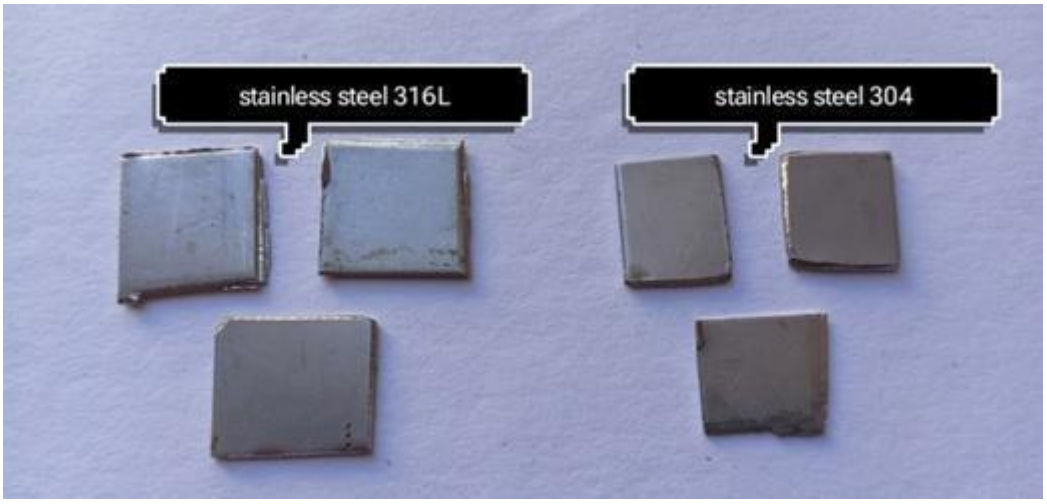

Figure 3.1. Specimens used in the study

The cutting process was performed using a shearing technique. Square specimens were cut from 316L stainless steel, as well as from 304 stainless steel. It is important to note that the 316L specimens were slightly bigger than the 304 ones. This size difference allowed us to clearly distinguish between the two types of specimens during subsequent analysis and processing steps.

3.2.2. Polishing

Polishing is a crucial finishing operation aims to remove surface imperfections such as cracks, porosity, inclusions, and geometric defects, particularly surface roughness. In this study, mechanical polishing is performed using a MECAPOL P230 polishing machine by PRESI**,** equipped with SiC abrasive papers given in Figure 3.2.

The polishing sequence involved successive use of abrasive papers with grit sizes of 400, 600, 800, 1200, and up to 2000, mounted on a horizontal rotating wheel operating at a constant speed. The polishing was carried out manually, with the specimen held perpendicular to the abrasive paper. Continuous water cooling was applied throughout the process to prevent overheating of the substrate.

The preparation continues with a final polishing, where the specimens are placed on rotating felt papers with alumina, until all scratches are removed and the surface acquires a mirror-like finish.

Figure 3.2. Polishing machine

3.2.3. Chemical Cleaning

The cleaning process aims to reduce contamination levels to acceptable limits, such contaminations generally originate from various sources, including:

- Residual impurities left after polishing and chemical etching;
- Interaction with the surrounding atmosphere;
- Residues from previous handling (such as oils or fingerprints);
- Dust particles and other similar pollutants.

To ensure that the specimens surfaces remain uncontaminated and free of any impurities that might hinder the effectiveness of the treatment or compromise results, the specimens were first cleaned in an ultrasonic bath of $C_3\ H_8\ O$ for 15 minutes as shown in Figure 3.3.

Additionally, direct contact with the specimen surface is avoided to prevent any further contamination.

Figure 3.3. Ultrasonic bath

3.3. Nitriding procedure

3.3.1. Equipment used in the treatment

The experimental setup used in this study enables nitriding by ion implantation, using a tubular furnace equipped with two electrodes that generate a glow discharge plasma. This system was designed and developed by Plasma and Applications team, part of the Ionized Media and Laser Division of CDTA. The process employed is illustrated in Figure 3.4**.**

Figure 3.4. Nitriding system by ion implantation of CDTA

3.3.2. Description of the nitriding furnace and of its components

The homemade designed nitriding furnace consists of a cylindrical steel chamber, a rotary vacuum pump capable of reaching a low pressure of approximately 1.10^{-2} mbar, a pressure gauge with its display unit, a gas inlet valve for N_2 through a capillary tube, and a type-C thermocouple for temperature measurement.

Figure 3.5 illustrates the layout and main components of the nitriding system.

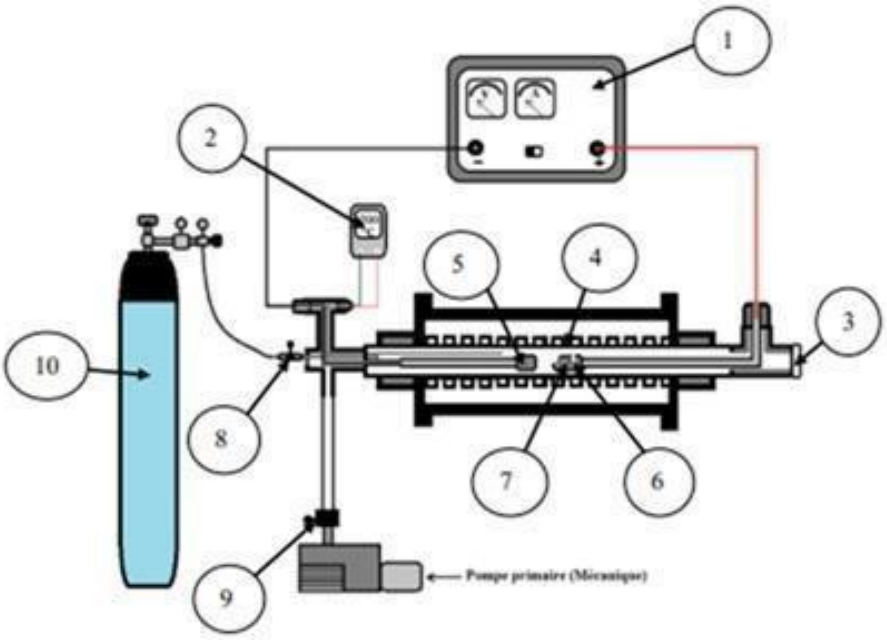

Figure 3.5. Schematic representative of the tubular furnace used: 1 – DC power supply. 2 – Thermometer. 3 – Viewing window. 4 – Heating element. 5 – Anode. 6 – Substrate holder (cathode). 7 – Substrate. 8 – Gas inlet valve. 9 – Valve. 10 – Nitrogen (N_2) gas cylinder

3.3.3. Nitriding Procedure and Main Processing Parameters

After preparing the required specimens, the nitriding process was initiated. Once the specimen was placed in the specimens holder and inserted into the furnace, the chamber is carefully sealed. The first step consists of evacuating the air inside the furnace. This first step has as aim to create a vacuum environment free of oxygen, residual gases, moisture, and other impurities. The internal pressure was reduced to approximately 0.1 mbar. The second step involved heating the furnace using its internal resistance element to gradually reach the desired treatment temperature. Once the target temperature was approached, a DC voltage was applied using the power supply to generate an internal current, while simultaneously allowing N_2 to enter the furnace, in gas nitriding, NH_3 is commonly used as the nitrogen-carrying gas. This causes the internal pressure to rise to approximately 2.5 mbar. At this stage, all the necessary conditions for nitriding process are established. The treatment is maintained under different solution treatments carried out within various temperatures for different holding times, followed by the cooling phase as a part of the annealing process. A successful initiation of the nitriding treatment can be seen by the appearance of a visible nitrogen plasma glow from the viewing window as shown in Figure 3.6.

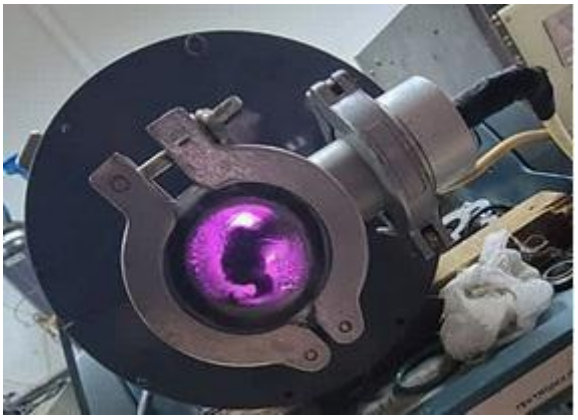

Figure 3.6. Glow of nitration-suspended nitrogen plasma

3.3.3.1. Solution Treatment

The nitriding process is governed through five key parameters: the applied power, working pressure, inter-electrode distance (target-to-substrate), substrate temperature, and deposition time. The process was carried out on specimens under different temperatures, each one is combined with different treatment durations. The specific nitriding conditions are summarized in the Table 3.1.

	Nitriding parameters	
specimens	**304**	**316L**
Tension (V)	500	
Current (mA)	20	
Pressure (mbar)	2.5	
Inter-electrodes space (mm)	40	
Gas	Nitrogen	
Duration (h)	2.5	4
Temperature (C°)	380	400

Table 3.1. Nitriding parameters

3.3.3.2. Annealing Treatment

After completing the nitriding process, the power source is turned off, the gas flow is stopped and the gas formed inside the furnace is suctioned using the suction pump, then the specimen is left in the furnace for a sufficient period of time to allow the temperature to gradually decrease. This cooling phase occurs naturally, without the influence of any external process, ensuring a slow and uniform temperature drop.

3.4. Characterization of the nitrided surfaces

To characterize the microstructure and identify the phases and precipitates present in the surface, both in the as-received specimens and the nitrided specimens , several characterization techniques were employed in this study. These methods enable to examine the evolution of the microstructure and mechanical properties. The characterization techniques used include:

- Metallographic analysis: using OM;
- Phase analysis: using XRD;
- Mechanical characterization: using nanoindentation test.

3.4.1. Metallographic Analysis by Optical Microscopy (OM)

OM was used to examine the microstructure and grain boundaries of the metal before and after the nitriding treatment. This technique allows for the evaluation of changes in grain size and morphology, enabling comparison of the microstructural evolution as a function of the applied treatment conditions.

Before proceeding with optical microscopy, the specimens were first mounted in resin to facilitate handling and prevent direct contact with the surface. Following this, the specimens surfaces were polished to ensure that the microstructural features could be clearly observed under a reflected light optical microscope as presented in Figure 3.7.

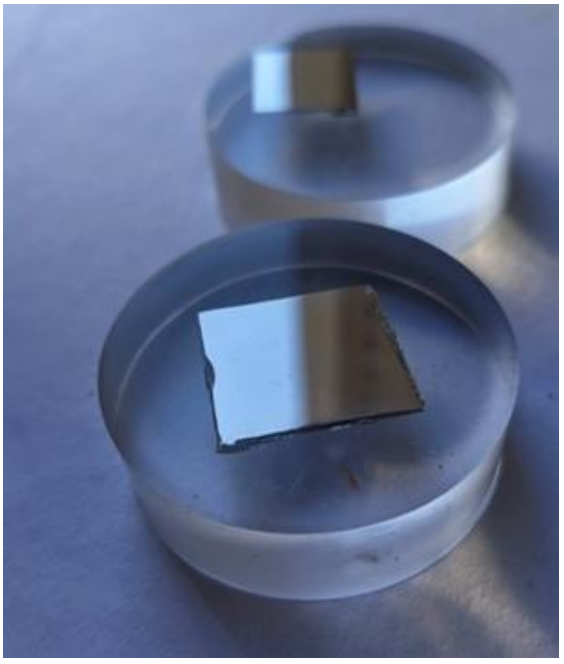

Figure 3.7. specimens after mounting and polishing

The specimens were then etched using various chemical reagents to reveal the microstructure. All metallographic preparations including mounting, polishing, and chemical etching were carried out at the CDTA laboratory. The observations were performed using a ZEISS AxioCam MRc 5 OM equipped with a digital camera connected to a computer for image acquisition and analysis (Figure 3.8).

Figure 3.8. Optical Microscopy (OM)

3.4.1.1 Mounting (Embedding)

In the mounting process, we used the MECAPRESS 2 device from PRESI (Figure 3.9), which operates with hot mounting. The clean and dry specimen is placed in the mounting press cylinder, after which transparent phenolic resin is added. A temperature of approximately 170 °C and a force of around 700 daN are applied for 7 minutes. The same duration 7 minutes is required for the cooling phase.

Mounting a specimen facilitates subsequent polishing while preserving its integrity. It also allows for safer and more convenient handling of the specimens .

Figure 3.9. Mounting machine

3.4.1.2 Chemical Etching

- To carry out this step and depending on what is aimed to be highlighted, the following reagents can be used for austenitic stainless steels:

- Marble's Reagent: 50 ml of HCl, 25 ml of $CuSO_4$, and 50 ml of distilled water. The etching duration is few seconds.
- 10% Oxalic Acid in H_2 O: the specimen is immersed in the solution, and a potential difference of 8V is applied between the specimen and an anode for approximately 50 seconds.

3.4.2 Phase Analysis by XRD

XRD is a non-destructive analytical technique that is essential for the in-depth analysis of crystalline materials. It allows for detailed examination of internal structures, identification of the existent phases, and determination of preferred crystallographic orientations, also known as texture. Furthermore, XRD enables the characterization of several structural parameters, such as the average crystallite size, degree of crystallinity, internal stresses and defects within the crystal lattice. This method thus, provides critical data for a better understanding of the physical and chemical properties of materials, contributing to the enhancement of their performance in a wide range of industrial and scientific applications [3.1].

The principle of XRD is based on irradiating the material to be analyzed with a monochromatic X-ray beam, typically emitted by a copper or cobalt target as can be seen in Figure 3.10. The intensity of the diffracted X-rays is then measured as a function of the orientation of the grains at the material's surface. When Bragg's conditions are met, the diffracted X-rays interfere constructively, producing diffraction peaks whose intensity is proportional to that of the reflected beam [3.2]. These diffraction peaks occur when the interplanar spacing d and the angle of incidence θ of the X-rays satisfy Bragg's Law [3.3]:

$$2dsin\theta = n\lambda$$

Where:

θ: the angle of incidence of the X-rays.

n: the order of diffraction.

λ: the wavelength of the X-rays.

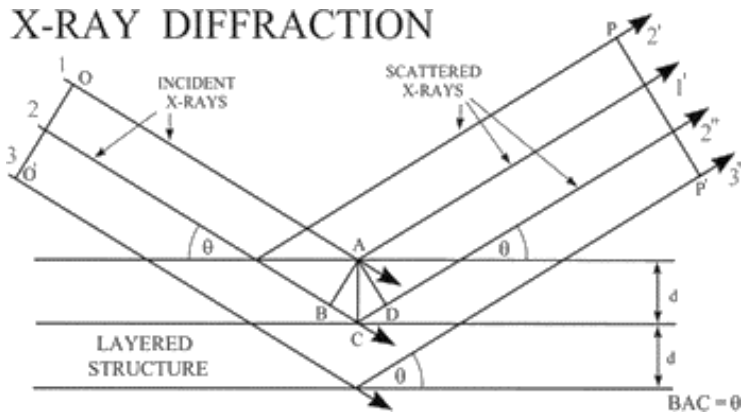

Figure 3.10. X-ray diffraction principle [3.4]

At the CDTA, the Bruker D8 Advance diffractometer shown in Figure 3.11 is equipped with a scintillation detector and a copper cathode X-ray source. Diffraction spectra are recorded at room temperature over an angular range from 20° to 100°, using grazing incidence mode.

- The specimen is mounted on a goniometric head.
- X-rays are generated by a copper target powered by a 40 kV, 40 mA generator.
- The radiation used corresponds to the Cu Kα line (λ = 1.54 Å), obtained using a germanium monochromator.
- Diffraction spectra are recorded over a 2θ angular range from 20° to 100°, with a step size of 0.05°.
- The identification of the phases present in the X-ray diffraction spectra has been carried out using EVA 5.0 software, and a PDF 2 database.

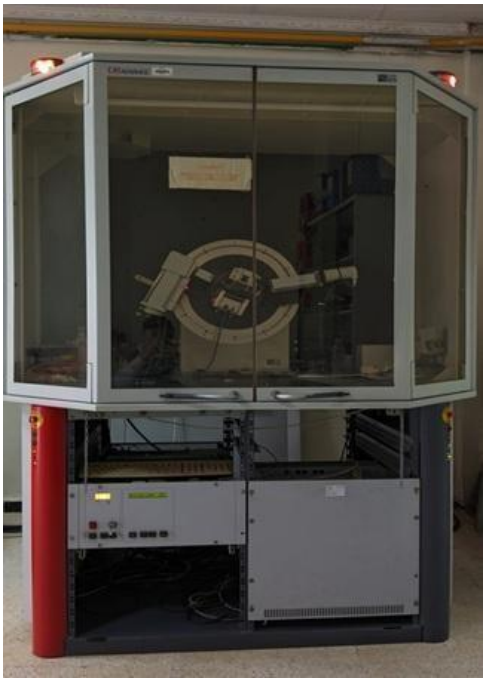

Figure 3.11. X-ray diffractometer used

3.4.3. Mechanical characterization by nanoindentation test

For certain applications, it is essential to apply low loads during indentation on the material. Traditionally, the measurement of the actual surface area of the residual imprint is performed using optical microscopy. However, this method becomes unsuitable when the indentation is too small to be reliably measured. To overcome these limitations, new analysis techniques emerged in the 1980s, leveraging technological advances that allow continuous recording of indentation depth as a function of applied load. The resulting curve, obtained during a loading-unloading cycle, is called the indentation curve. The hardness and elastic modulus of the material are then extracted from the unloading segment of this curve, following the analysis method proposed by Oliver and Pharr. [3.5].

When conducting indentation profile measurements, meticulous specimen preparation is crucial. Mechanical polishing can introduce plastic deformation, so it is necessary to thoroughly remove any work-hardened layers. The polishing process must maintain the crystalline structure of the specimen near the surface under analysis while effectively eliminating surface oxidation and contamination, all without causing additional work hardening or excessive roughness. To achieve this, the specimens were processed following the standard polishing protocol, which includes removing the work-hardened layer after each step. The equipment used in is a Berkovich type indenter integrated within a CSM system.

Figure 3.12. Nano-indentation dispositif

The two main properties measured are the elastic modulus E and hardness H. The most commonly used model for calculating the modulus and hardness is that developed by Oliver

and Pharr [3.6]. The contact area Ac between the indenter and the specimen is defined for the measurement of hardness and elastic modulus by the following relation:

$$Ac = 24{,}56.\ hc$$

$$hc = \mathrm{hmax} - \varepsilon.\frac{\mathrm{Fmax}}{\mathrm{s}}$$

Hardness determination:

$$H = \frac{\mathrm{Fmax}}{\mathrm{Ac}}$$

Determination of Young s module :

$$S = \frac{\mathrm{df}}{\mathrm{dh}} = 2\sqrt{\pi}\,.\,\mathrm{Er}\,.\sqrt{\mathrm{Ac}}$$

$$\frac{1}{\mathrm{Er}} = \frac{1 - vi^2}{\mathrm{Ei}} + \frac{1 - v^2}{\mathrm{E}}$$

Where:

Er: reduced elastic modulus.

Ei: elastic modulus of the indenter.

E: elastic modulus of the specimen.

vi: Poisson's ratio of the indenter.

v: Poisson's ratio of the specimen.

3.5. Conclusion

As a conclusion, this chapter deals with the experimental procedures that is applied throughout the study. It is listed how stainless steel specimens (AISI 304 and AISI 316L) were prepared for nitriding treatment and subsequent annealing processes, all performed under controlled conditions. The combined use of OM and XRD enabled a thorough investigation of nitridation-induced microstructural and phase transitions. Furthermore, mechanical properties were systematically assessed through a nanoscale serration test, providing a comprehensive understanding of the effects of treatments on materials. This empirical basis paves the way for the detailed analysis and discussion presented in the following chapters.

References

[3.1] https://www.eaglabs.fr/ « Diffraction des rayons X, analyse XRD ».

[3.2] Fouaz. LEKOUI, Elaboration et Caractérisation d 'un système en couches minces fonctionnelles Zn-Ag-M g-O, Thèse de doctorat, Université 20 Août 1955, Skikda, 2019.

[3.3] H.W. Kim, N.H. Kim, Annealing effect for structural morphology of ZnO film on SiO 2 substrates, Sci. Semicond. Process, 2004, vol. 7, p. 6-1.

[3.4] https://physicsopenlab.org/wp-content/uploads/2018/01/xrd6.jpg.

[3.5] W. Oliver et G. Pharr, "Improved technique for determining hardness and elastic modulus using load and displacement sensing indentation experiments," Journal of Materials Research, vol. 7, 1992, p. 1564-1580.

[3.6] Olivier. Warren C, Pharr. Georges M, Measurement of hardness and elastic modulus by instrumented indentation: Advances in understanding and refinements to methodology, Journal of materials research, 2004, vol. 19, no 1, p. 3-20.

Chapter 4

Results and Discussion

Chapter 4: Results and Discussion

4.1. Introduction

This final chapter is devoted to a comparative analysis of the structural, mechanical, and electrochemical behavior of two austenitic stainless steels, AISI 304 and AISI 316L, in their untreated (raw) state and after plasma nitriding at low temperature. The aim is to evaluate the effectiveness of the nitriding treatment in enhancing the surface performance of both alloys under identical conditions. Structural modifications were first investigated using X-Ray Diffraction (XRD), which revealed significant broadening and shifting of the diffraction peaks, indicating the formation of expanded austenite (γN) and compressive residual stresses in both steels, more pronounced in the 316L one. The mechanical properties were evaluated through nanoindentation tests, where both materials exhibited a substantial increase in surface hardness post-nitriding, with 304 stainless steel showing a relatively greater hardening effect due to a denser diffusion layer. Electrochemical performance was assessed using potentiodynamic polarization (Tafel) and Electrochemical Impedance Spectroscopy (EIS). While the corrosion resistance of nitrided 316L stainless steel improved markedly, highlited by higher polarization resistance and a capacitive response in EIS. The nitrided 304 stainless steel showed a decrease in corrosion performance, likely due to microstructural discontinuities or unstable passive film formation. This comprehensive analysis provides a clear treatment, and highlights the importance of alloy composition in determining nitriding outcomes understanding of the different responses of 304 and 316L stainless steels to the same surface

4.2. Structural properties

4.2.1. XRD analysis

4.2.1.1. XRD analysis of AISI 304 stainless steel before and after plasma nitriding

The XRD patterns presented in Figure 4.1 correspond to specimens of AISI 304 stainless steel, analysed before and after being subjected to plasma nitriding at 380 °C for 2.5 hours. The untreated specimen (black curve) exhibits three sharp and well-defined diffraction peaks located at approximately $2\theta \approx 43.5°$, 50.5° and 74.5° which correspond to the (111), (200),

and (220)

crystallographic planes of austenite (γ-Fe) with a Face-Centered Cubic (FCC) structure. These are in good agreement with the standard diffraction data from JCPDS card No. 00-033-0397 [4.1].

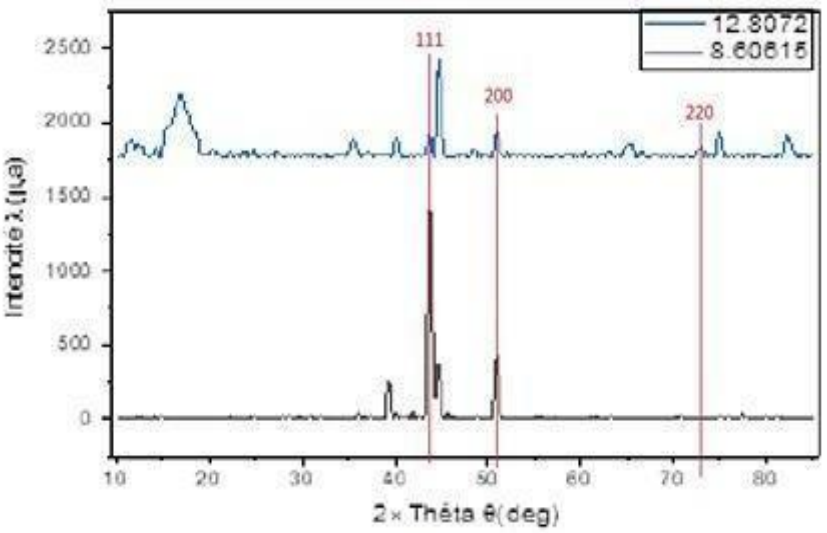

Figure 4.1. XRD pattern of AISI 304 stainless steel

After plasma nitriding (blue curve), noticeable structural modifications can be observed in the XRD pattern, such as:

- The appearance of additional peaks at lower angles (~22° and ~27°).
- The emergence of new peaks at ~ 37°, 58°, and 63°.
- Broadening and slight shifting of the original austenite peaks toward lower angles.

These changes can be explained as follows:

1. Formation of Expanded Austenite (γN):

At the relatively low processing temperature of 380 °C, full phase transformation does not occur. Instead, nitrogen atoms diffuse interstitially into the FCC lattice of austenite without forming separate nitride phases. This leads to lattice expansion, inducing internal compressive stresses and resulting in new diffraction peaks at lower 2θ angles. This metastable phase, known as expanded austenite (γN), is characterized by significantly enhanced surface hardness and corrosion resistance [4.2, 4.3].

2. Possible Formation of Nitrides (CrN, Fe_4 N):

Although 380 °C is relatively low for the precipitation of stable nitrides, the presence of peaks around 37°, 58°, and 63° could indicate the initial formation of fine CrN or Fe-based nitrides (e.g., Fe_2 -$_3$ N or Fe_4 N), particularly under high nitrogen saturation and extended treatment time. These nitrides contribute to improving wear and corrosion resistance in the treated surface layer [4.4, 4.5].

3. Broadening and Shifting of peaks after Plasma Nitriding

In addition to the formation of new diffraction peaks after plasma nitriding, noticeable broadening and low-angle shifting of the original peaks was observed in the XRD pattern of AISI 304 stainless steel treated at 380 °C for 2.5 hours. These changes are associated with modifications in the crystal lattice due to nitrogen diffusion and are summarized in Table 5.1:

Crystallographic Interpretation	**Observation**	**After Nitriding**	**Original Peak Position (2θ)**
Expansion of the FCC lattice due to interstitial nitrogen absorption → formation of expanded austenite (γN) [4.2, 4.3].	Broadening and Low-angle shift	≈ 43.2°	≈ 43.5° (γ-Fe, (111))
Internal compressive stresses and refinement of surface grain size (nanoscale crystallites) [4.3, 4.5].	Significant broadening	≈ 50.2°	≈ 50.5° (γ-Fe, (200))
Mild distortions in the FCC lattice while retaining its original structure [4.5].	Slight broadening and minor shift	≈ 74.1°	≈ 74.5° (γ-Fe, (220))

Table 4.1. Modifications in the crystal lattice due to nitrogen diffusion

4.2.1.2. XRD analysis of AISI 316L stainless steel before and after plasma nitriding

XRD analysis was performed on AISI 316L stainless steel specimens to study the structural changes induced by plasma nitriding. The treatment was conducted at 390 °C for 4 hours under controlled low-temperature conditions. The resulting diffraction patterns before and after nitriding reveal significant changes in crystal structure and lattice parameters due to nitrogen diffusion.

The XRD pattern of the untreated specimen displays distinct peaks corresponding to the austenitic (γ) phase, which is characterized by a Face-Centered Cubic (FCC) lattice. The main diffraction peaks were observed in Figure 4.2.

- $2\theta \approx 43.6°$, corresponding to the (111) plane.
- $2\theta \approx 50.7°$, corresponding to the (200) plane.
- $2\theta \approx 74.6°$, corresponding to the (220) plane.

These peaks are in agreement with the standard ICDD reference for AISI 316L stainless steel (PDF Card No. 31-0619) [4.6]. The absence of secondary phases or nitrides confirms the phase purity and stability of the austenitic structure in the untreated material.

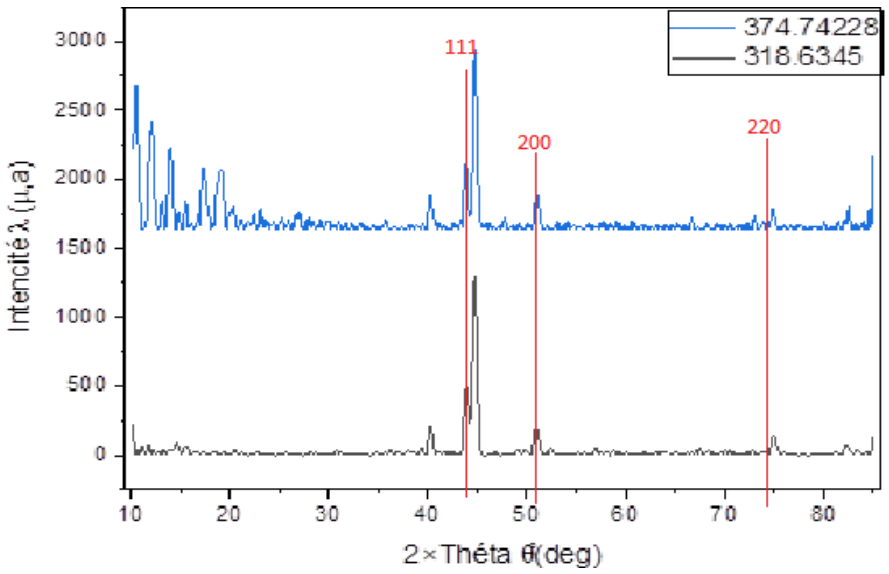

Figure 4.2. XRD pattern of AISI 316 stainless steel

1. Formation of Expanded Austenite (γ□ / S-Phase):

After plasma nitriding at 390 °C, significant changes were observed in the diffraction pattern, indicating the formation of expanded austenite (γ□), also known as the S-phase. This metastable phase results from the supersaturation of nitrogen in the austenitic lattice without the precipitation of nitrides [4.7]. The following structural modifications were detected:

- A shift of the (111) peak from 43.6° to approximately 42-43°, indicating lattice expansion due to nitrogen interstitials [4.7, 4.8].
- A similar shift of the (200) peak to around 49-50°, also associated with compressive stress in the expanded lattice [4.8].
- Noticeable peak broadening, which is attributed to increased dislocation density, stacking faults, and compressive residual stresses [4.9].

2. Non-formation of nitrides (CrN, Fe_4 N):

No CrN or Cr_2 N peaks were detected (typically observed at ~37.6° and 43.2°, respectively), suggesting that no chromium nitride precipitates formed during the low-temperature nitriding process [4.7, 4.10]. This is favorable, as it maintains the corrosion resistance of stainless steel by preventing chromium depletion.

The XRD analysis confirms the successful formation of expanded austenite (γ□) in the surface layer of AISI 316L following plasma nitriding at 390 °C for 4 hours. The peak shifts toward lower 2θ angles and the broadening of diffraction peaks strongly indicate nitrogen uptake and lattice expansion, in line with interstitial solid solution behavior [4.7-4.9]. Importantly, the

absence of CrN and Cr_2 N phases ensures that corrosion resistance is preserved, as no chromium depletion occurred [4.10].

These findings validate the efficacy of low-temperature plasma nitriding in enhancing surface hardness and wear resistance without compromising the passivation properties of austenitic stainless steels.

4.2.2. Optical microscope analyse

Optical microscopy was carried out to investigate the microstructural features of AISI 304 (Figure 4.3) and AISI 316L (Figure 4.4**)** austenitic stainless steels. The micrographs revealed a fully austenitic structure in both alloys, characterized by elongated or equiaxed grains with noticeable twinning, which is indicative of the Face-Centered Cubic (FCC) crystal structure [4.11]. It is unfortunate that we could not take pictures of the specimens after nitruration for technical reasons, but the pictures we took of the normal condition confirmed to us the nature of the specimens and the distribution of austenite.

In AISI 304 stainless steel specimens (Figure 4.3), the microstructure is dominated by homogeneous austenitic grains, confirming the stability of the austenite phase and the absence of significant secondary phases under the given processing conditions [4.12].

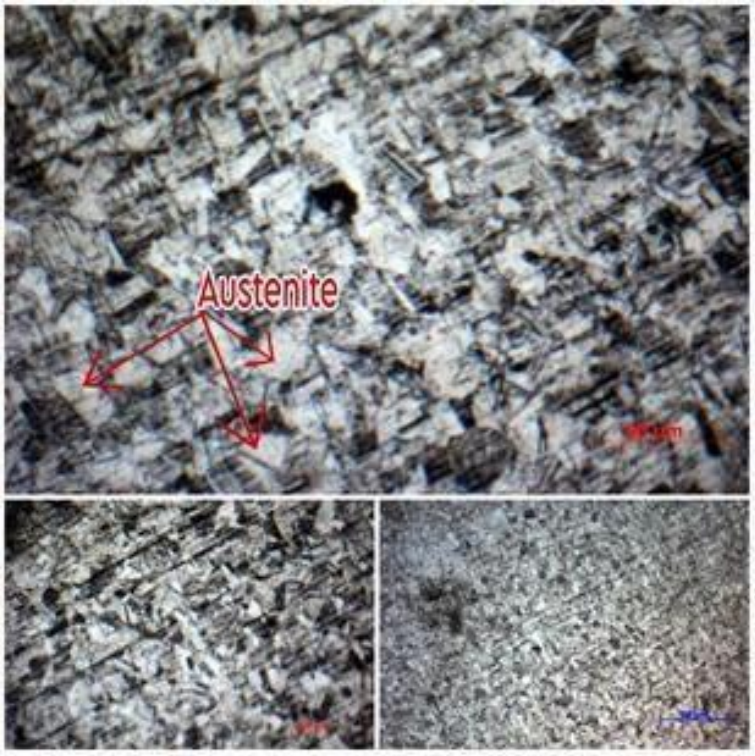

Figure 4.3. Microstructure observation of AISI 304 stainless steel specimen under optical microscope

In contrast, the AISI 316L specimen (Figure 4.4) also exhibited an austenitic matrix, but with the presence of dark carbide precipitates, mainly located along the grain boundaries and within the

grains. These precipitates are most likely chromium-rich carbides of the $M_{23}C_6$ type, which typically form during thermal exposure such as welding or slow cooling [4.13]. These carbides can locally deplete chromium in the surrounding matrix, potentially reducing corrosion resistance (sensitization) and impacting mechanical properties [4.14].

The grain size and phase distribution observed in the 316L stainless steel specimen is consistent with its low carbon content (≤0.03 wt%), which minimizes carbide formation compared to standard 316 stainless steels [4.15]. All images were taken at different magnifications (50 to 100 µm scale) to highlight both general grain morphology and fine features such as carbides and twin boundaries.

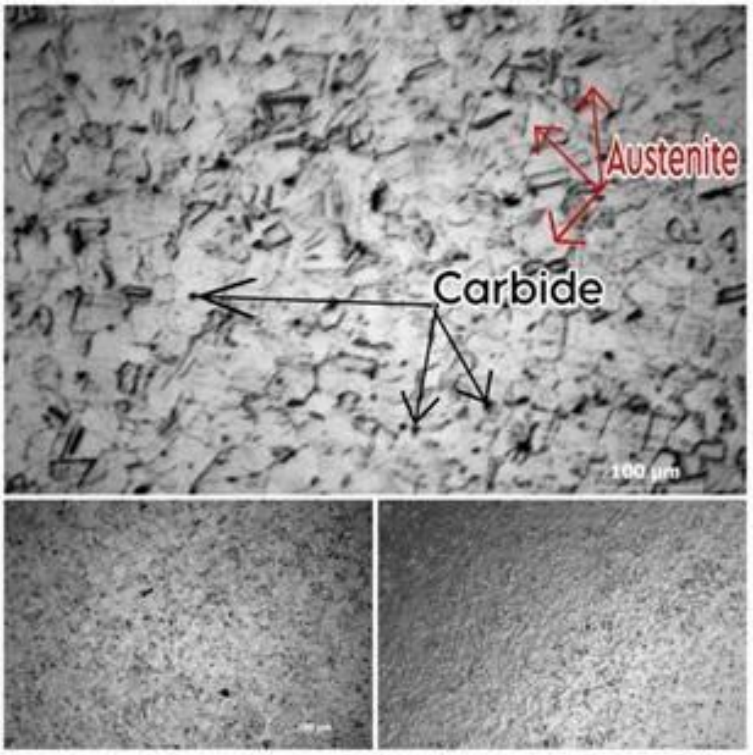

Figure 4.4. Microstructure observation of AISI 316L stainless steel specimen under optical microscope

4.3. Nanoindentation test of AISI 316L and AISI 304 stainless steels

Nanoindentation testing was conducted on stainless steel specimens of types AISI 316L and AISI 304 using a sharp diamond indenter, in order to evaluate the effect of plasma nitriding process on surface mechanical properties. The resulting curves illustrate the relationship between applied load (in mN) and penetration depth (in nm) during both the loading and unloading phases, enabling the assessment of surface hardness, resistance to plastic deformation, and elastic recovery.

4.3.1. AISI 316L behavior before and after nitriding

The untreated AISI 316L specimen exhibited a relatively deep indentation under an applied load of approximately 100 mN, indicating low surface hardness and a high tendency for plastic deformation. In contrast, the nitrided AISI 316L specimen showed a clear reduction in penetration depth (~1070 nm compared to ~1100 nm) and a steeper unloading curve (Figure 4.5), reflecting a notable improvement in both surface hardness and elastic recovery. This enhancement is primarily attributed to the formation of expanded austenite (γ□), a nitrogen-enriched metastable phase that forms in the surface layer during plasma nitriding without the precipitation of hard nitrides [4.7, 4.8]. Consequently, plasma nitriding significantly increases the resistance of AISI 316L to mechanical indentation and deformation, thereby enhancing its wear and scratch resistance.

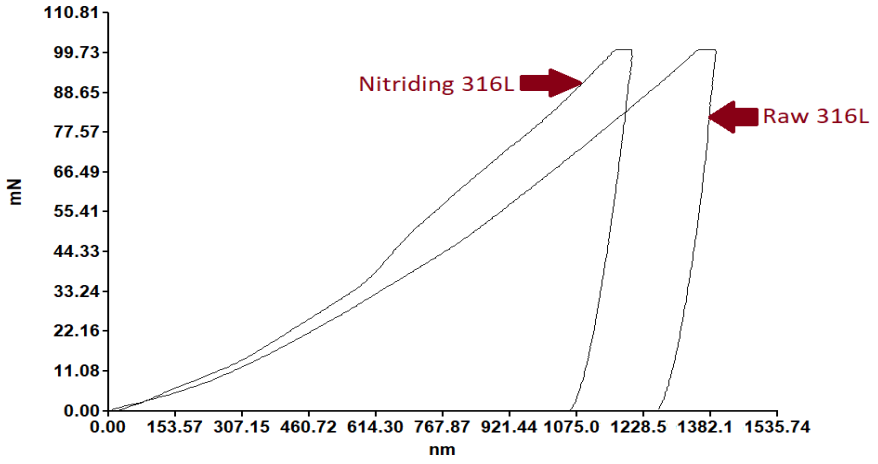

Figure 4.5. Load – unload curves of raw 316L and nitrided 316L stainless steels

4.3.2. AISI 304 behavior before and after Nitriding

The untreated AISI 304 specimen exhibited a deeper indentation (~1150 nm), indicating relatively low surface hardness and limited resistance to localized plastic deformation. Following plasma nitriding, the treated AISI 304 specimen (Figure 4.6) demonstrated a clear improvement, with reduced penetration depth (~1100 nm) and enhanced elastic recovery. This improvement is attributed to nitrogen enrichment in the surface layer and the formation of expanded austenite (γ□), without the undesirable precipitation of chromium nitrides that could compromise corrosion resistance [4.7, 4.9]. Similar to AISI 316L, plasma nitriding significantly enhanced the mechanical performance of AISI 304 by increasing its resistance to microplastic deformation.

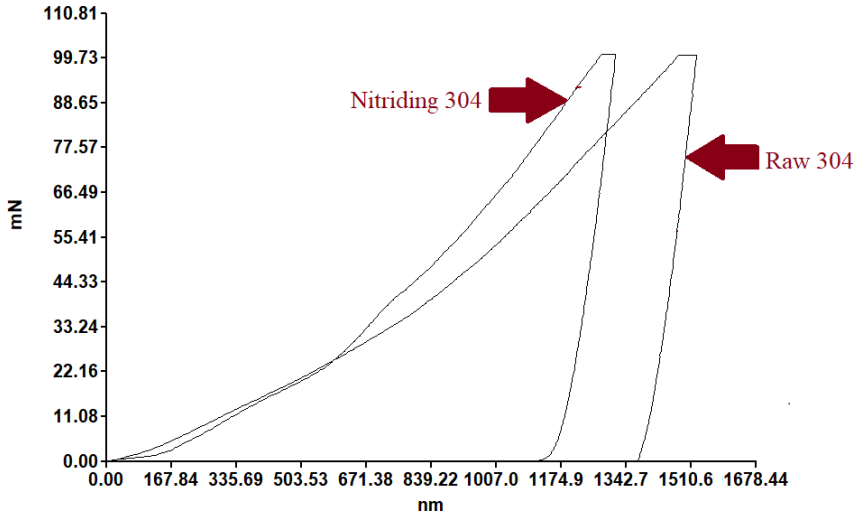

Figure 4.6. Load – unload curves of raw 304 and nitrided 304 stainless steels

Table 4.2 compares between nanoindentation results of AISI 316L and AISI 304 before and after plasma nitriding.

Material	Specimens Condition	Maximum Indentation Depth (nm)	Maximum Load (mN)	Mechanical Behavior	Conclusion
AISI 316L	Before nitriding	~1100	~100	Deep indentation – significant plastic deformation	Low surface hardness
	After nitriding	~1070	~100	Improved elastic recovery	Increased hardness and deformation resistance
AISI 304	Before nitriding	~1150	~100	Deeper penetration – lower surface resistance	Relatively low surface hardness
	After Nitriding	~1100	~100	Improved response – reduced depth and higher recovery	Higher hardness and enhanced wear resistance

Table 4.2. Compares between nanoindentation results of AISI 316L and AISI 304 before and after plasma nitriding

Nanoindentation results clearly demonstrate that low-temperature plasma nitriding is an effective technique for improving the surface mechanical properties of austenitic stainless steels. This treatment leads to:

- Increased surface hardness.
- Improved resistance to indentation and micro-deformation.
- Enhanced elastic recovery.
- All without compromising corrosion resistance or altering the base microstructure.

4.4. Tafel and EIS tests

4.4.1. Tafel test

4.4.1.1. Tafel test for AISI 304 stainless steel

Electrochemical corrosion behavior of AISI 304 stainless steel was evaluated using Tafel polarization curves before (Figure 4.7) and after plasma nitriding (Figure 4.8). The raw AISI 304 specimen exhibited a corrosion potential E_{corr} of E_{corr} = –28.689 mV and a very low corrosion current density I_{corr} of I_{corr} = 7.756 nA, indicating excellent resistance to uniform corrosion in the tested environment. The anodic and cathodic Tafel slopes were 53.911 mV/dec and 38.2 mV/dec, respectively, suggesting a relatively stable electrochemical interface and passive behavior. After plasma nitriding, the corrosion potential shifted significantly to more negative value of E_{corr} = –306.868 mV, and the corrosion current density increased substantially to I_{corr} = 3.971 µA. This shift indicates a reduction in corrosion resistance under open circuit conditions, likely due to changes in the surface chemistry or increased surface activity. However, the anodic Tafel slope of the nitrided specimen decreased to 33.102 mV/dec, indicating an altered anodic reaction mechanism, while the cathodic slope increased to 53.761 mV/dec, suggesting slower cathodic kinetics.

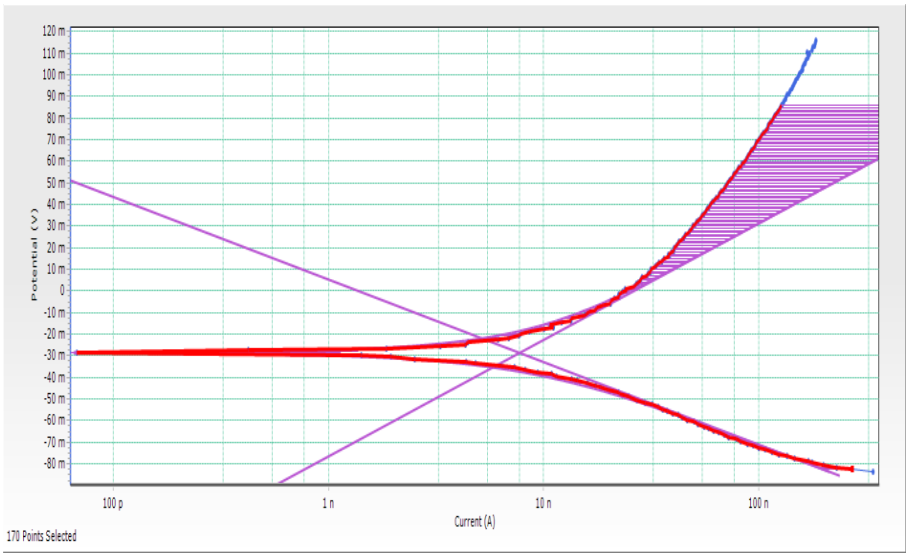

Figure 4.7. Tafel polarization curves of AISI 304 stainless steel before plasma nitriding

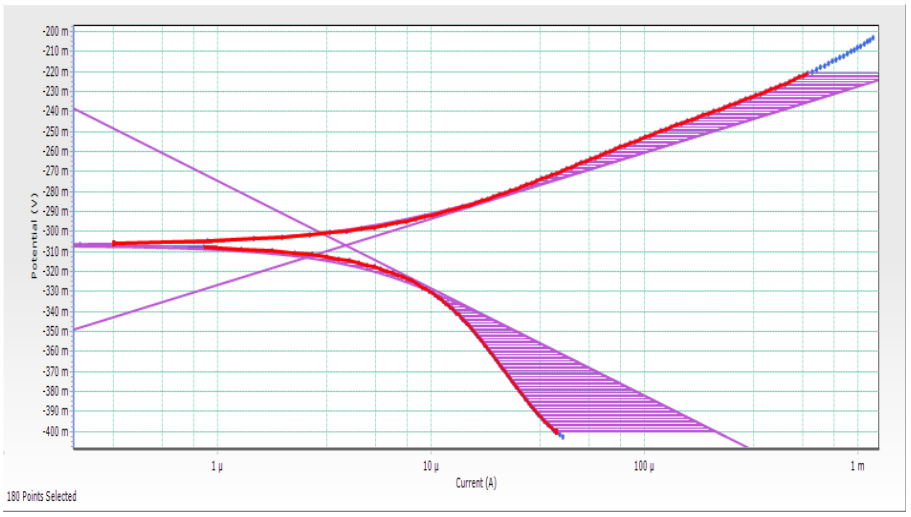

Figure 4.8. Tafel polarization curves of AISI 304 stainless steel after plasma nitriding

Despite the higher corrosion current density, the nitrided surface may offer improved localized corrosion resistance and enhanced surface hardness due to nitrogen diffusion and nitride formation. This demonstrates the trade-off between electrochemical corrosion performance and surface durability, commonly observed in surface-modified stainless steels [4.16, 4.17, 4.13] (Figure 4.9).

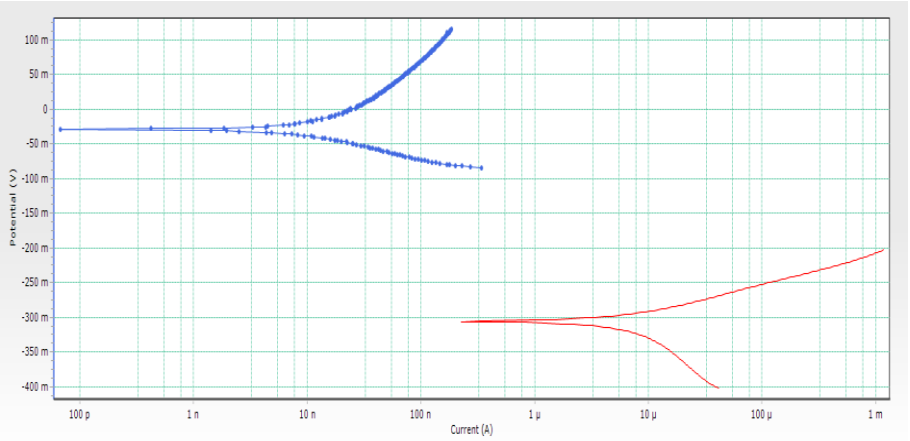

Figure 4.9. Trade-off between electrochemical corrosion performance and surface durability of 316L stainless steel

4.4.1.2. Tafel test for AISI 316L stainless steel

The Tafel polarization curves for AISI 316L stainless steel in acidic media illustrate the electrochemical differences between the raw (Figure 4.10) and plasma-nitrided conditions (Figure 4.11).

The untreated 316L (blue curve) displayed a corrosion potential of E_{corr} = –40.51 mV and a very low corrosion current density of I_{corr}=10.507 nA, indicating high resistance to general corrosion. The anodic and cathodic Tafel slopes were 72.306 mV/dec and 26.44 mV/dec, respectively, showing that the passive film remains stable over a wide potential range. In contrast, the nitrided specimen (red curve) exhibited a significantly more negative

corrosion

potential of E_{corr} = –316.198 mV and a substantially higher corrosion current density of I_{corr} = 6.692 µA, reflecting increased electrochemical activity at the surface. This behavior is attributed to surface modification by nitrogen diffusion and the formation of nitrided layers, which can disrupt passive film formation but improve hardness and wear resistance. The anodic Tafel slope decreased to 42.585 mV/dec, indicating faster anodic reaction kinetics, while the cathodic slope increased to 63.738 mV/dec, suggesting slowed cathodic reactions.

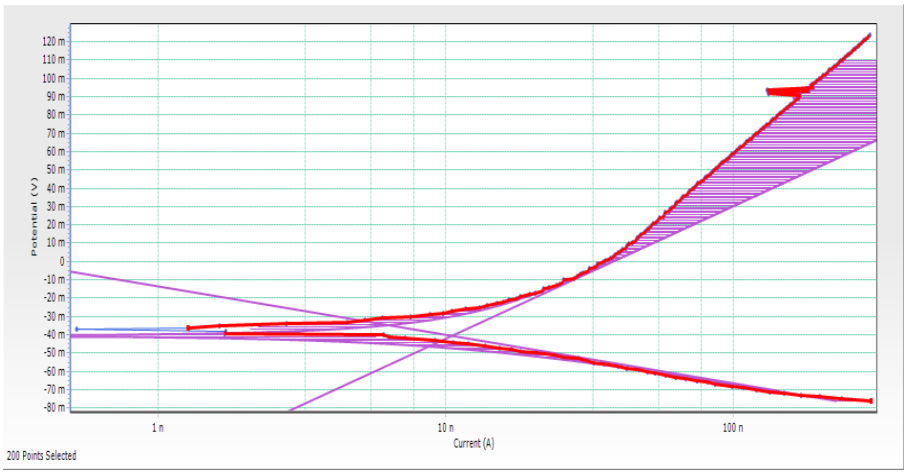

Figure 4.10. Tafel polarization curves of AISI 316L stainless steel before plasma nitriding

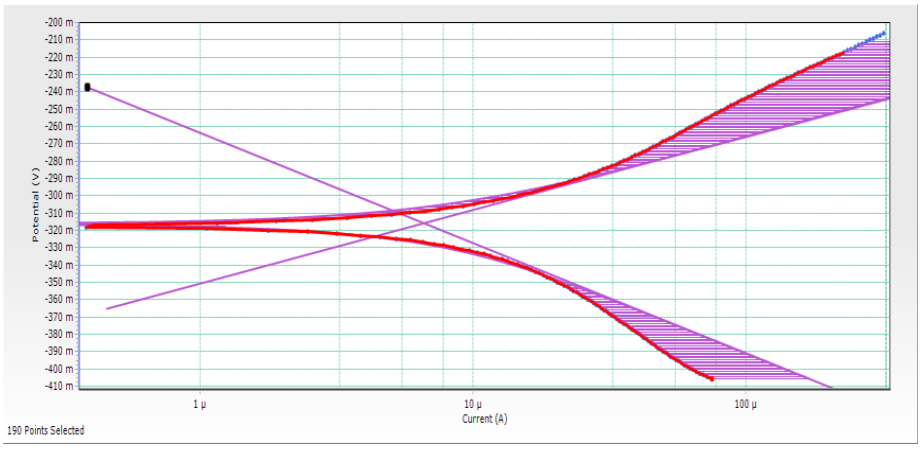

Figure 4.11: Tafel polarization curves of AISI 316L stainless steel after plasma nitriding

Despite a reduction in general corrosion resistance, nitriding enhances mechanical performance, making the material suitable for applications where surface durability is prioritized over corrosion rate [4.16, 4.17, 4.13] (Figure 4.12).

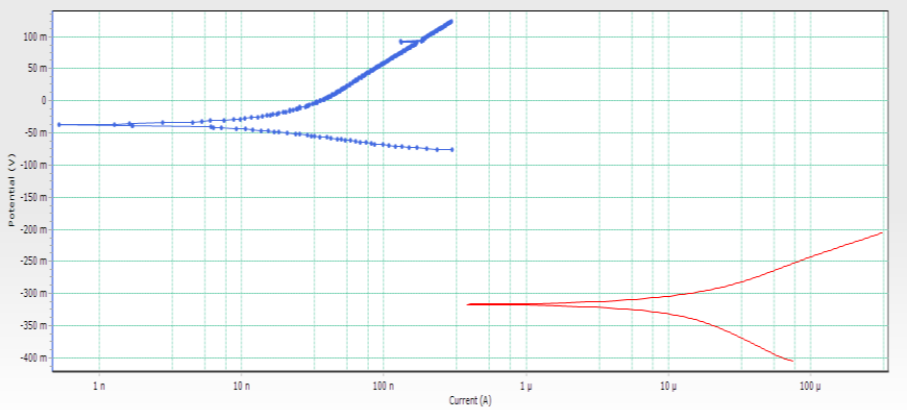

Figure 4.12. Trade-off between electrochemical corrosion performance and surface durability of 316L stainless steel

4.4.2. EIS test

4.4.2.1. EIS test for AISI 304 stainless steel

Electrochemical Impedance Spectroscopy (EIS) was employed to evaluate the corrosion behavior of AISI 304 stainless steel before (Figure 4.13) and after plasma nitriding (Figure 4.14).

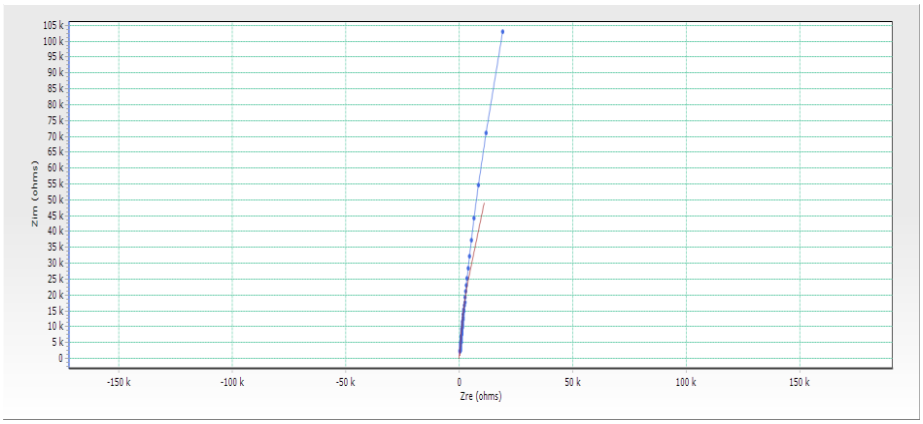

Figure 4.13. Corrosion behavior of AISI 304 stainless steel before plasma nitriding

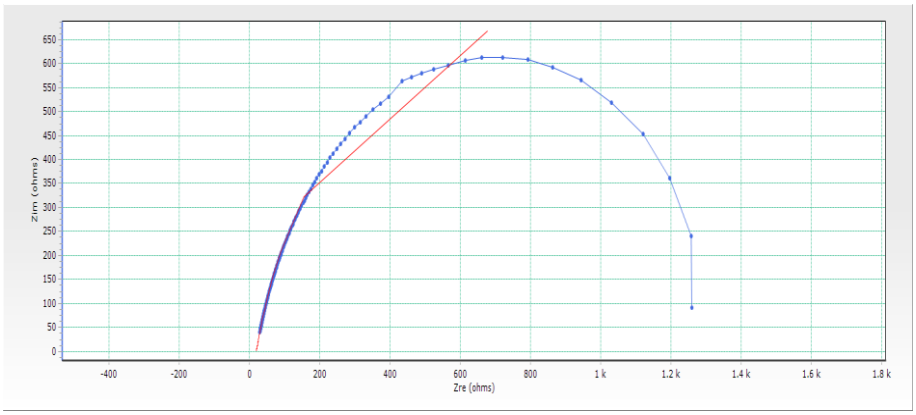

Figure 4.14. The corrosion behavior of AISI 304 stainless steel after plasma nitriding

The Nyquist plot in Figure 4.15 reveals a significant difference in impedance response between the untreated (304L blanc) and nitrided (304L nitruré) specimens . The untreated specimen exhibits

a large semicircular arc, indicating a high charge transfer resistance (Rct), characteristic of a stable and protective passive film. In contrast, the nitrided specimen shows a drastically smaller arc, reflecting a reduced Rct and suggesting a compromised corrosion resistance. This behavior may be attributed to the formation of a thin or porous nitride layer, which can allow electrolyte penetration and hinder the reformation of the native $Cr_2 O_3$ passive layer. Additionally, nitrogen- induced changes in surface chemistry could disrupt the passive behavior typically observed in austenitic stainless steels. These results align with findings in the literature, where low- temperature nitriding, although beneficial for surface hardness, can negatively affect corrosion performance if not properly optimized [4.18-4.20]. Therefore, while nitriding improved certain mechanical properties, it appears to have diminished the electrochemical stability of the material in the tested environment.

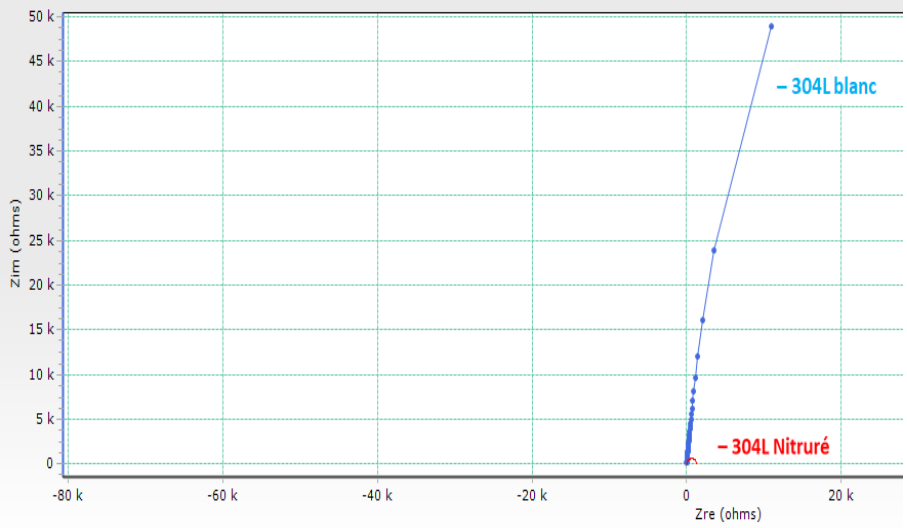

Figure 4.15. difference in impedance response between the untreated (304L blanc) and nitrided (304L nitruré) specimens

4.4.2.2. EIS test for AISI 316L stainless steel

Electrochemical Impedance Spectroscopy (EIS) was conducted to compare the corrosion behavior of AISI 316L stainless steel before (Figure 4.16) and after plasma nitriding (Figure 4.17).

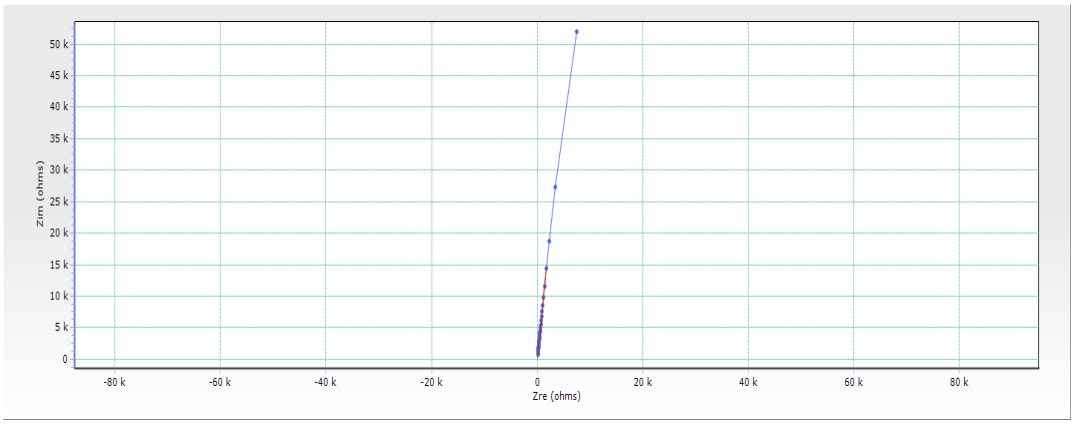

Figure 4.16. Corrosion behavior of AISI 316L stainless steel before plasma nitriding

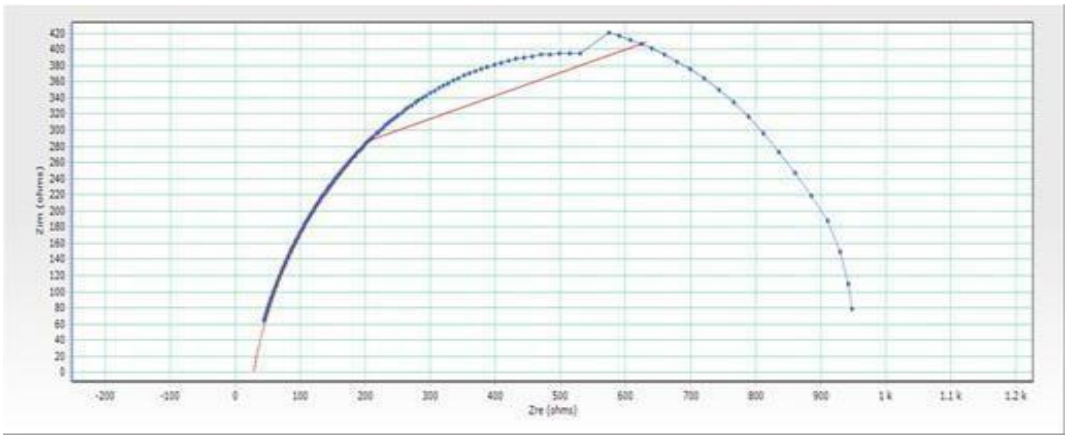

Figure 4.17. the corrosion behavior of AISI 316L stainless steel after plasma nitriding.

As shown in the Nyquist plot in Figure 4.18**,** low charge transfer resistance (Rct). This reflects a moderately protective passive film inherent to 316L stainless steel. However, after nitriding, the specimen (316L nitruré) exhibits a nearly vertical line in the high-impedance region, a characteristic of capacitive behavior and excellent surface protection. This significant increase in impedance suggests that the nitrided layer acts as an effective barrier to charge transfer and electrolyte penetration. Such improvement can be attributed to the formation of a dense, uniform nitrogen-enriched layer (such as expanded austenite, γN) and/or chromium nitride phases, which enhance corrosion resistance by reinforcing the passive film [4.18, 4.20, 4.21]. These findings confirm the beneficial effect of low-temperature plasma nitriding on the electrochemical stability of AISI 316L stainless steel.

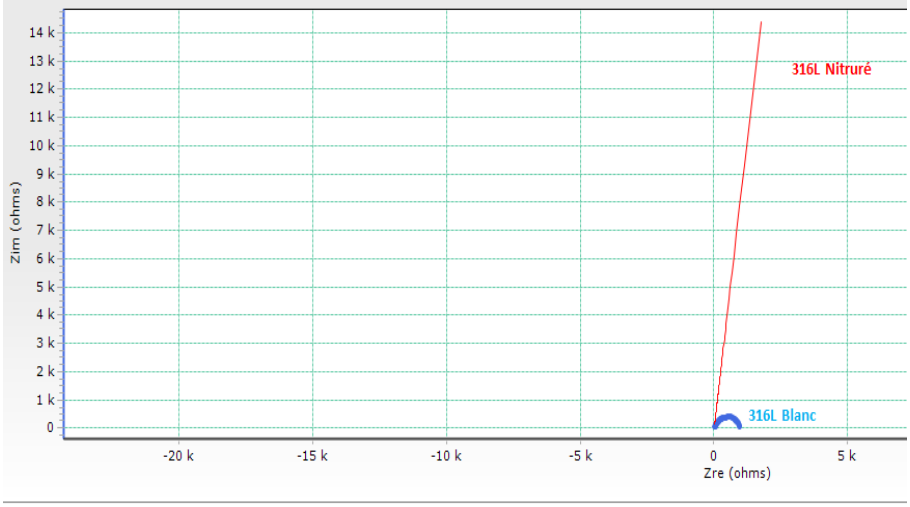

Figure 4.18. the low charge transfer resistance (Rct)

4.5. Conclusion

This chapter provided a comprehensive comparison of AISI 304L and 316L stainless steels in their untreated and plasma-nitrided states, with a focus on structural, mechanical, and electrochemical properties. X-ray diffraction analyses confirmed the formation of expanded austenite (γN) in both nitrided alloys, as evidenced by the peak broadening and shift to lower angles. These structural modifications correlated with improved surface hardness in both steels, as demonstrated by nanoindentation testing, where nitrided specimens exhibited significantly increased hardness and elastic modulus compared to their raw counterparts.

However, the electrochemical behavior revealed contrasting effects of nitriding on the two alloys, while 316L showed a clear improvement in corrosion resistance after nitriding, demonstrated by higher polarization resistance in Tafel plots and a strong capacitive response in EIS measurements. The nitrided 304L exhibited reduced electrochemical performance. This was likely due to the formation of an unstable or porous nitride layer that compromised the passive film's integrity. These findings highlight the critical role of alloy composition and microstructure in determining the effectiveness of plasma nitriding treatments.

In summary, low-temperature plasma nitriding effectively enhanced both the mechanical and corrosion resistance of 316L stainless steel. In contrast, while 304L benefited from improved surface hardness, its corrosion behavior deteriorated under the same treatment conditions. This underlines the need for alloy-specific optimization of nitriding parameters to ensure balanced improvements in mechanical and electrochemical performance.

References

[4.1] nternational Centre for Diffraction Data (ICDD). (1978). Powder Diffraction File, Card No. 00-033-0397. Swarthmore, PA: Joint Committee on Powder Diffraction Standards.

[4.2] Mingolo, N., Tschiptschin, A., & Pinedo, C. E. (2006). Structure and properties of expanded austenite formed during low temperature plasma nitriding of an AISI 316L austenitic stainless steel. Surface and Coatings Technology, 201(13), 4971–4978.
ResearchGate

[4.3] Menthe, E., Rie, K. T., et al. (1999). "Improvement of the mechanical properties of austenitic stainless steel after plasma nitriding." Surface and Coatings Technology, 116–119, 199–204.

[4.4] Dong, H. (2010)."Surface engineering of metallic biomaterials." Surface Engineering, 26(3), 177–185.

[4.5] Sun, Y., & Bell, T. (1998). "Plasma surface engineering of low alloy steel." Materials Science and Engineering: A, 140(3), 419–434.

[4.6] ICDD PDF Card No. 31-0619 – Standard pattern for AISI 316L Austenite.

[4.7] Christiansen, T., Somers, M. A. J. Low temperature surface hardening of stainless steel. ScriptaMaterialia, 2005, 53(3), 335–340.

[4.8] Sun, Y. Kinetics of low temperature plasma nitriding of austenitic stainless steel. Surface and Coatings Technology, 2005, 200(5–6), 1514–1520.

[4.9] Beltowska-Lehman, E., et al. Structure and properties of the nitrided layer formed on AISI 316L steel. Coatings, 2020, 10(10), 984. https://doi.org/10.3390/coatings10100984

[4.10] Mandl, S. Plasma nitriding of stainless steels. Surface and Coatings Technology, 2020.

[4.11] Davis, J.R. (Ed.) (1994). Stainless Steels.ASM International. Chapter on Austenitic Stainless Steels – describes FCC structure and twinning in austenite.

[4.12] Callister, W.D. &Rethwisch, D.G. (2018). Materials Science and Engineering: An Introduction. 10th ed. Wiley. – Explanation of microstructural stability in FCC austenite.

[4.13] Sedriks, A.J. (1996). Corrosion of Stainless Steels.2nd ed., Wiley. – Description of carbide ($M_{23}C_6$) formation and its locations.

[4.14] Lo, K.H., Shek, C.H., & Lai, J.K.L. (2009)."Recent developments in stainless steels." Materials Science and Engineering: R: Reports, 65(4–6), 39–104. – Impact of carbides on sensitization and corrosion.

[4.15] ASTM A240/A240M-20 – Specification for chromium and chromium-nickel stainless steel plate, sheet, and strip for pressure vessels and general applications (defines maximum carbon content in 316L as ≤ 0.03%).

[4.16] ASTM G102-89(2015), Standard Practice for Calculation of Corrosion Rates and Related Information from Electrochemical Measurements, ASTM International, 2015.

[4.17] M. A. El-Sherik, "Electrochemical Techniques for Corrosion Engineering," in Trends in Oil and Gas Corrosion Research and Technologies, Woodhead Publishing, 2017, pp. 335–368.

[4.17] M. A. El-Sherik, "Electrochemical Techniques for Corrosion Engineering," in Trends in Oil and Gas Corrosion Research and Technologies, Woodhead Publishing, 2017.

[4.18] Li, C.X., Bell, T. (2006). Corrosion properties of active screen plasma nitrided 316 austenitic stainless steel. Surface and Coatings Technology, 201(6), 2791–2796.

[4.19] Souza, R.C., Ariza, E., Silva, M.B. et al. (2009).Corrosion behavior of plasma nitrided AISI 316L stainless steel in NaCl solution. Corrosion Science, 51(3), 642–649.

[4.20] Sun, Y. (2005). A study of the corrosion behaviour of nitrogen plasma implanted 316L stainless steel. Surface and Coatings Technology, 193(1–3), 73–79.

[4.21] Menthe, E., Bulak, A., Olfe, J., Zimmermann, A., Rie, K.T. (2000). Improvement of the mechanical properties of austenitic stainless steel after plasma nitriding. Surface and Coatings Technology, 133–134, 259–263.

General Conclusion

The work presented in this thesis focuses on The effect of plasma nitriding at low temperatures up to 400°C on the surface properties of AISI 304 and AISI 316L austenitic stainless steels, successfully confirming the formation of expanded austenite (γN) in both alloys, as evidenced by diffraction peak broadening and shifting towards lower angles in the X-Ray Diffraction (XRD) analyses. This structural modification correlated directly with improved mechanical performance, as nanoindentation testing demonstrated that the nitriding treatment substantially increased surface hardness and enhanced elastic recovery for both 304 and 316L grades compared to their untreated states. Crucially, the electrochemical evaluation revealed contrasting results that highlighted the critical role of alloy composition: for AISI 316L, nitriding significantly enhanced corrosion resistance, which was characterized by a strongly capacitive response in Electrochemical Impedance Spectroscopy (EIS) and the layer acting as an effective charge transfer barrier, a favorable outcome partially attributed to the non-formation of chromium nitride precipitates during the low-temperature process. Conversely, the same treatment conditions led to a reduction in the electrochemical stability of AISI 304, demonstrated by a significant negative shift in the corrosion potential (Ecorr) and a reduced charge transfer resistance observed in the EIS Nyquist plot, suggesting the formation of an unstable or porous nitride layer that compromised the integrity of the passive film. Consequently, while low-temperature plasma nitriding effectively improved the mechanical properties of both steels, a balanced enhancement of both mechanical and corrosion resistance was only achieved in AISI 316L.